Applied Surface Science 399 (2017) 682–701

Contents lists available at ScienceDirect

Applied Surface Science

journal homepage: www.elsevier.com/locate/apsusc

Full Length Article

Synthesis of calcium-phosphorous doped TiO_2 nanotubes by anodization and reverse polarization: A promising strategy for an efficient biofunctional implant surface

Sofia A. Alves[a,b,*], Sweetu B. Patel[b,c], Cortino Sukotjo[b,d], Mathew T. Mathew[b,e,f], Paulo N. Filho[g,j], Jean-Pierre Celis[h], Luís A. Rocha[a,g,j], Tolou Shokuhfar[b,c,i]

[a] CMEMS – Center of MicroElectroMechanical Systems, Department of Mechanical Engineering, University of Minho, 4800-058 Guimarães, Portugal
[b] IBTN/US – American Branch of the Institute of Biomaterials, Tribocorrosion and Nanomedicine, UIC College of Dentistry, 60612 Chicago, IL, USA
[c] Department of Mechanical Engineering, Michigan Technological University, 49931 Houghton, MI, USA
[d] Departmenmt of Restorative Dentistry, University of Illinois at Chicago, 60612 Chicago, IL, USA
[e] Department of Orthopedic Surgery, Rush University Medical Center, 60612 Chicago, IL, USA
[f] Department of Biomedical Science, UIC School of Medicine at Rockford, 61107 Rockford, IL, USA
[g] IBTN/Br – Brazilian Branch of the Institute of Biomaterials, Tribocorrosion and Nanomedicine, UNESP – Universidade Estadual Paulista, Faculdade de Ciências, 17033-360 Bauru, São Paulo, Brazil
[h] Department of Materials Engineering, KU Leuven, 3001 Leuven, Belgium
[i] Department of Bioengineering, University of Illinois at Chicago, 60607 Chicago, IL, USA
[j] Faculdade de Ciências, Departamento de Física, UNESP - Universidade Estadual Paulista, 17033-360 Bauru, São Paulo, Brasil

ARTICLE INFO

Article history:
Received 10 November 2016
Received in revised form 6 December 2016
Accepted 14 December 2016
Available online 14 December 2016

Keywords:
Bio-functionalization
Anodization
Reverse polarization
TiO_2 nanotubes
Calcium-phosphorous surface
Osseointegrated implants

ABSTRACT

The modification of surface features such as nano-morphology/topography and chemistry have been employed in the attempt to design titanium oxide surfaces able to overcome the current dental implants failures. The main goal of this study is the synthesis of bone-like structured titanium dioxide (TiO_2) nanotubes enriched with Calcium (Ca) and Phosphorous (P) able to enhance osteoblastic cell functions and, simultaneously, display an improved corrosion behavior. To achieve the main goal, TiO_2 nanotubes were synthetized and doped with Ca and P by means of a novel methodology which relied, firstly, on the synthesis of TiO_2 nanotubes by anodization of titanium in an organic electrolyte followed by reverse polarization and/or anodization, in an aqueous electrolyte. Results show that hydrophilic bone-like structured TiO_2 nanotubes were successfully synthesized presenting a highly ordered nano-morphology characterized by non-uniform diameters. The chemical analysis of such nanotubes confirmed the presence of $CaCO_3$, $Ca_3(PO_4)_2$, $CaHPO_4$ and CaO compounds. The nanotube surfaces submitted to reverse polarization, presented an improved cell adhesion and proliferation compared to smooth titanium. Furthermore, these surfaces displayed a significantly lower passive current in artificial saliva, and so, potential to minimize their bio-degradation through corrosion processes. This study addresses a very simple and promising multidisciplinary approach bringing new insights for the development of novel methodologies to improve the outcome of osseointegrated implants.

1. Introduction

Dental implants are widely used to replace tooth loss due to decay, trauma or periodontal diseases [1]. Additionally, market demand has been increasing within the past years, both due to the aging of the population and to the success that dental implant therapies have reached [2], improving the life quality of people. However, a significant number of dental implant failures (1–20%) have still been described [3], which is the subject of main concern since revision surgeries are painful to patients and very expensive to companies. The growing demand along with the high failure rates further increase the interest on the improvement of quality, efficiency and lifetime of dental implants.

Commercially pure titanium (cp-Ti) and its alloys are the metallic materials most commonly used in dental implants due to their superior biocompatibility, mechanical properties and high

* Corresponding author at: CMEMS – Center of MicroElectroMechanical Systems, Department of Mechanical Engineering, University of Minho, 4800-058 Guimarães, Portugal.
E-mail address: sofiafonso@msn.com (S.A. Alves).

http://dx.doi.org/10.1016/j.apsusc.2016.12.105
0169-4332/

corrosion resistance [4–8]. However, despite the outstanding properties, implant failures are often caused by the lack of a stable implant anchorage provided by direct bone-to-implant contact (i.e. osseointegration) [9]. Also, the release of metallic wear debris and corrosion products to implant surroundings, is a main problem.

Aiming to overcome the current difficulties, researchers have been working worldwide on the improvement of implant surface features through multidisciplinary approaches. Over the past years, it has been widely reported that implant surface topography, morphology, chemical composition and surface energy have a critical influence on cell adhesion, proliferation, differentiation and osteoblastic extracellular matrix expression [10–13], which are cellular functions dictating the success rate of osseointegration [14–17]. Therefore, surface modification treatments have been carried out in a concentrated effort to construct suitable biomimetic interfacial microenvironments able to improve cell-materials interactions generating bone in a faster and improved osseointegration process [18–22]. In particular, special attention is being devoted to the modification of Ti features at a nanoscale level by mimicking the micro/nanostructures of natural bone [3,19–21,23]. Among the various surface modification techniques, electrochemical anodization of Ti has usually been used to synthesize biologically-inspired nanostructures [24–26]. In particular, vertically aligned TiO_2 nanotubes created on Ti, have become increasingly popular to enhance adhesion, growth and accelerate the osteo-differenciation of mesenchymal stem cells [19]. Oh et al. [27] indicated that the presence of nanotube structures on Ti produced an interlocked cell structure created due to the improved adhesion of osteoblasts to nanotubular Ti oxide film, with the filopodia of the growing cells going into the nanotube pores. Furthermore, such nanotubular Ti structure led to a significant acceleration in the growth rate of osteoblasts cells by up to 400%. Beyond the excellent osteoblast adhesion and proliferation promoted by TiO_2 nanotubes, these structures have been suggested as a way to avoid the formation of fibrous tissue [21]. The occurrence of metallic implant corrosion is also an issue of main importance. Despite the high corrosion resistance of Ti materials, they are not inert to corrosive attack in presence of the aggressive biological environment [28,29]. Corrosion ions/products may be released from the metallic implant to surroundings tissues, causing inflammation and local toxicity, resulting in tissue damage, implant loosening and need of a new surgery [19,30–32]. Thus, the design of implant surfaces able to resist to corrosion attack is also an issue of main significance and, electrochemical anodization appears as a very promising way to address it. It is known that implant surface features significantly influence the electrochemical stability of the metallic implant when in contact with simulated body fluids. Very interestingly, in particular, TiO_2 nanotubes have also shown potential to prevent long term implant failure due to bio-corrosion [32,33]. This behavior is related to the anodization of Ti which is characterized by the growth of a compact oxide film on its surface formed through a natural and intrinsic chemical bond between the oxide and Ti substrate [21,34].

In an attempt to develop new strategies for the construction of biomimetic systems, various modifications have already been employed to TiO_2 nanotubes through thermal oxidation, coating deposition, hydrothermal treatments in saturated solutions for nanotube doping and drug-loading [10,35]. Beyond the wide number of treatments already employed, no one has explored anodization as a possible way to modify the nanotube features and provide them multiple functionalities. Electrochemical anodization is a very versatile technique which allows the handling of the chemistry of the native TiO_2 layer by the incorporation of species such as calcium (Ca) and phosphorus (P), natively present in bone [36]. The benefits of Ca- and P-enriched Ti surfaces by anodization have already been demonstrated both *in vitro* by improving cell attachment, adhesion, and proliferation and *in vivo*, by accelerating the primary osteogenic response [13,37,38]. Additionally, Ca- and P-based Ti surfaces synthesized by anodization, have shown improved corrosion and wear resistant properties than untreated Ti [39–42].

In the present study, reverse polarization and electrochemical anodization of TiO_2 nanotubes were explored as a new strategy for the synthesis of multifunctional implant surfaces that can enhance osteoblastic cell functions and simultaneously, minimize their degradation by corrosion. To achieve this goal, bone-like structured TiO_2 nanotubes were synthetized and doped with Ca and P (Ca/P-doped TiO_2 nanotubes) by reverse polarization and/or anodization processes in an aqueous electrolyte containing Ca and P (Ca/P-electrolyte). Ca/P-doped nanotubes were deeply characterized regarding their surface features as well as their biological and electrochemical properties.

2. Experimental details

2.1. Surface pre-treatment

Discs of commercially pure titanium (cp-Ti) grade 2 (American Society for Testing of Materials – Grade 2) (MacMaster-carr, IL, USA) of 15 mm diameter and 2 mm thickness were used as substrates used in this study. Firstly, the samples were ground with a series of silicon carbide (SiC) sandpapers #240, #320, #400, #600 and #800 (Carbimet 2, Buehler, Lake Bluff, IL, USA). Afterwards, the TexMet polishing cloth (TexMet Polishing Cloth, Beuhler, Lake Bluff, IL, USA) with diamond paste (MetaDi 9-μm, Beuhler, Lake Bluff, IL, USA) and lubricant fluid (MetaDi Fluid, Beuhler, Lake Bluff, IL, USA), followed by the Chemomet polishing cloth (Chemomet, Buheler, Lake Bluff, IL, USA) with colloidal silica polishing suspension (MasterMed, Buehler, Lake Bluff, IL, USA), were used to polish cp-Ti surfaces until mirror finishing. Lastly, all the samples were ultrasonically cleaned in ethanol (10 min), distilled (DI) water (5 min) and finally, they were dried at room temperature. These smooth cp-Ti samples were used as a control group in the present study and they were named as Ti.

2.2. Synthesis of well-ordered TiO_2 nanotubes

The nanotubes were obtained by anodization using a two-electrode set-up with Ti samples and a graphite rod as the working and counter electrodes, respectively. Both electrodes were connected to a power supply (Keithley 2400 SourceMeter, Cleveland, OH, USA) and immersed in an electrolyte constituted by Ethylene Glycol (EG) (Ethylene Glycol, Fisher Scientific, Pittsburgh, PA, USA), 0.3 wt.% ammonium fluoride (NH_4F) (Ammonium Fluoride, Sigma-Aldrich, St. Louis, MO, USA) and 3 vol.% DI water. The distance between the working and the counter electrode was approximately 2 cm, and the electrolyte was continuously stirred at room temperature (22–24 °C). The nanotubes were produced by a two-step anodizing process. The first anodization was carried out upon Ti surfaces at a constant voltage of 60 V for 1 h. The resulting nanotubes were then removed by ultrasonication in isopropanol for 15 min and afterwards these substrates were rinsed in DI water and dried in air. The second anodizing step was then performed on these surfaces for 30 min under the same conditions, leading to the growth of well-ordered nanotubes named as NT. After this final step, NT surfaces were immediately gently rinsed with DI water and dried at room temperature.

2.3. Bio-functionalization of well-ordered TiO_2 nanotubes with Ca and P

TiO_2 nanotubes were submitted to functionalization treatments by reverse polarization and/or anodization, aiming at the incorpo-

ration of Ca and P species in its structure. In a first approach, the NT surfaces were used as the working electrode, and a graphite rod was the counter electrode. A constant voltage of 100 V was applied for 30 min between both electrodes immersed in an electrolyte composed of 0.35 M calcium acetate (CaA) (Calcium acetate monohydrate, Sigma-Aldrich, St. Louis, MO, USA) and 0.04 M β-glycerolphosphate (β-GP) (β-glycerolphosphate disodium salt pentahydrate, Sigma-Aldrich, St. Louis, MO, USA), named as Ca/P-electrolyte. These specimens were named as NT-Ca/P. As a second approach, aiming to improve the bioactivity of TiO_2 nanotubes, a reverse polarization step was also carried out. For that, right before the anodization in the Ca/P-electrolyte, the polarity of the electrodes was inverted. By this way, NT samples became the cathode and graphite rod became the anode. Reverse polarization was applied during 10 s at 20 V. After this time, the polarity of the electrodes was inverted again, and a constant voltage of 100 V was applied for 30 min with the samples immersed in the same electrolyte. These samples were named as NT-RP-Ca/P. The nanotubular samples subjected to functionalization treatments in Ca/P-electrolyte were named as Ca/P-doped nanotubes.

2.4. Surface characterization

The morphology of Ti, NT, NT-Ca/P and NT-RP-Ca/P surfaces was analyzed by Field Emission Scanning Electron Microscopy (FESEM) (JSM-6320F, JEOL, Musashino 3-chome Akishima Tokyo, Japan). For imaging, the different groups of samples were mounted on an aluminum stub with double sided conductive carbon tape. FESEM images from the top of the surfaces were obtained with 10,000× and 40,000× magnifications. The morphology of the cross-sections of the different groups of samples was also characterized by FESEM. Before FESEM observations, the cross-sections were polished using the standard metallographic preparation protocol described in Section 2.1. The FESEM images were obtained with magnification of 5000×. From FESEM pictures, nanotube features such as diameter, wall thickness, and the length were measured using ImageJ software.

The surface topography of the samples was assessed via White-light Interferometry (NewView 6300, Zygo Corporation, Middlefield, Connecticut, USA). The average roughness (R_a) was measured, and a 3D profile of each surface was generated using an imaging analysis tool (Metropro 8.1.5), which is associated with the interferometer. The R_a values were calculated from a minimum of three independent measurements.

The elemental composition of the different groups of surfaces was determined by Energy-dispersive X-ray spectroscopy (EDS) using a JEOL JSM-6320F detector incorporated into the FESEM system. Furthermore, the binding states of the elements detected on nanotubular surfaces were investigated by X-ray Photoelectron Spectroscopy (XPS) by using Kratos AXIS-165 surface analysis system. To find out the functional groups present on Ti surfaces after functionalization treatments, Fourier Transform Infrared Spectroscopy (FTIR, Nicolet, Madison, WI, USA) was carried out. The range of FTIR spectra was of 4000 cm^{-1}–400 cm^{-1} with 1 cm^{-1} resolution and 512 scans. Ti samples were used as a control.

Finally, water contact angle (WCA) measurements of the different groups of surfaces were performed by the sessile drop method using a contact angle measurement apparatus (CA Goniometer, Rame'-Hart NRL, Succasunna, NJ, USA) equipped with a camera imaging system. Prior to WCA measurements, the samples were cleaned with DI water followed by N_2 gas drying, at room temperature. For WCA, a 5 μL droplet of DI water was suspended on the surface using a micro-syringe (Hamilton, Reno, NV, USA). Pictures were collected from the camera, and the contact angle between the droplet and the substrate surface was calculated by ImageJ software. The WCA measurements were performed in triplicate, within a maximum period of 48 h after nanotubular surfaces fabrication.

2.5. Electrochemical studies

Potentiodynamic studies were carried out in artificial saliva (AS) at 37 °C. The composition of AS is described elsewhere [43]. The samples were fixed in an electrochemical cell with the desired surface facing upwards. For these experiments, a three-electrode setup was used where the Ti samples were the working electrode, graphite was the counter electrode, and a saturated calomel electrode (SCE, 0.244 V *vs.* SHE) the reference electrode. Firstly, the samples were immersed AS (volume = 10 mL) for 3600 s for open circuit potential (OCP) stabilization. Afterwards, potentiodynamic polarization tests were carried out from −0.8 V until 1.8 V *vs.* SCE. The scan rate used for potentiodynamic polarization was 2 mV s^{-1}. The corrosion parameter evaluated from potentyodinamic polarization scan was the passive current (I_{pass}), which was determined from current measurements within the passivation region of the potentiodynamic scan. The experiments were carried out in triplicate for each group.

The electrochemical measurements were carried out with a potentiostat (Gamry Instrument, Reference 600) coupled to the framework software (Gamry Instrument) for monitoring the electrochemical data.

2.6. Biological characterization of Ca/P-doped TiO_2 nanotubes

2.6.1. Cell culture

MG-63 human osteosarcoma cells (ATCC number CRL-1427™) were used for cell-material interactions studies. MG-63 cells were cultured in standard plates (Treated cell culture dish, Falcon, Corning, NY, USA) in Dulbecco's High Glucose Modified Eagles Medium (DMEM High Glucose, HyClone, GE Healthcare Life Sciences, UT, USA). The culture medium was supplemented with 10% (V/V) of Fetal Bovine Serum (FBS, Gibco, Life Technologies, NY, USA) and 1% (V/V) of antibiotic (Anti-Anti, Gibco, Life Technologies, NY, USA) in a humidified atmosphere with 5% carbon dioxide (CO_2), at 37 °C. The culture medium was changed every three days. At 80% confluence, the adherent cells were enzymatically detached from the bottom of the culture dishes using 0.05% (1X) trypsin (HyClone, GE Healthcare Life Sciences, UT, USA) and counted in a hemocytometer (Bright-Line, Hausser Scientific, PA, USA).

Before cell culture, all the materials were sterilized by immersion in ethanol 70% (V/V) for 30 min and placed into standard 24-well culture plates (Falcon, Corning, NY, USA). Furthermore, it is important to highlight that *in vitro* studies were conducted in samples with the maximum of one week of aging, to avoid its effect on surface wettability.

2.6.2. Cell morphology

The morphology of adhered MG-63 cells on materials surface was observed by FESEM. For this, one mL of MG-63 cell suspension (2×10^4 cell/mL) was seeded on Ti, NT, NT-Ca/P and NT-RP-Ca/P samples, which were placed into 24-well culture plates. After one and six days of incubation at 37 °C in a 5% CO_2 humidified atmosphere, the morphology of MG-63 cells was observed by FESEM. During incubation period, the culture medium was changed every three days. For FESEM observation, firstly, the cells were washed in phosphate-buffered saline (PBS, HyClone, GE Healthcare Life Sciences, UT, USA) and fixed with 2% glutaraldehyde in sodium cacodylate buffer, pH 7.4 (Electron Microscopy Sciences, Pennsylvania, USA). Then, the cells were dehydrated using graded ethanol solutions from 35% (V/V) to 100% (V/V) followed by immersion in 100% (V/V) hexamethyldisilazane (HMDS). The samples lasted 10 min in each ethanol and HMDS solution. Finally, the samples

Table 1
Diameter, wall-thickness and length of TiO_2 nanotube arrays on NT, NT-Ca/P and NT-RP-Ca/P samples.

Group	NT diameter (nm ± SD)	NT wall-thickness (nm ± SD)	NT length (μm ± SD)
NT	74.1 ± 13.7	19 ± 4.6	12 ± 0.4
NT-Ca/P	67.2 ± 13.4	17.9 ± 3.7	13 ± 1.6
NT-RP-Ca/P	59.8 ± 12.3	18.5 ± 3.2	5.5 ± 0.1*

(*) significantly different from NT and NT-Ca/P; $p < 0.001$.

were placed onto an aluminum stub and sputter coated with gold. Then, the samples were observed by FESEM (JSM-6320F, JEOL, Musashino 3-chome Akishima Tokyo) with the acceleration voltage of 10 kV.

The cell morphology was also investigated by fluorescence microscopy. For this purpose, Ti, NT, NT-Ca/P and NT-RP-Ca/P samples were placed in 24-well culture plates and 1 mL of MG-63 cell suspension (2×10^4 cell/mL) was cultured on each surface. After one and six days of culture, MG-63 cells were labeled for actin filaments of cytoskeleton and nucleus, for subsequent observation in the fluorescence microscope. For this, the cells were washed in PBS and fixed with a solution of 3.7% (V/V) formaldehyde (Ricca Chemical Company, TX, USA) in PBS for 20 min. Afterwards, cells were washed in PBS and permeabilized with 0.1% triton-X (Triton X-100, Fisher Scientific, Pittsburgh, PA, USA) in PBS, for 15 min. Then, 1 mL of PBS was added to each well and, ActinRed™ 555 ReadyProbes™ reagent (Molecular Probes, Life Technologies, NY, USA) was added to each well according to manufacturer instructions, for actin filaments labeling. After cytoskeleton staining, cells were washed in PBS and NucBlue Fixed Cell Stain ReadyProbes™ reagent (Molecular Probes, Life Technologies, NY, USA) was added to each well, according to manufacturer instructions. Finally, cells were washed with PBS solution and maintained in this solution for fluorescence microscopy observation.

2.6.3. Metabolic activity

Firstly, Ti, NT, NT-Ca/P and NT-RP-Ca/P samples were placed in 24-well culture plates (triplicates were used per condition). Afterwards, 1 mL of MG-63 cell suspension (4×10^4 cell/mL) was seeded on the surface of each sample and additionally, the cells were also cultured on the wells of the culture plates, for cell viability control. Then, the culture plates were placed in a 5% CO_2 atmosphere at 37 °C for one and six days. The culture medium was changed every three days.

After each incubation period, the cellular metabolic activity was evaluated by measuring the mitochondrial dehydrogenase activity through MTT (3-(4,5-dimethyl-2-thiazolyl)-2,5-diphenyl-2H-tetrazolium bromide) reduction assay. The MTT assay allows the assessment of living and metabolically active cells by their reduction activity of the yellow MTT into soluble purple formazan product by mitochondrial dehydrogenase [11,15,44]. After one and six days of culture, the cells were incubated with MTT (0.5 mg/mL, Sigma-Aldrich, MO, USA) for 4 h at 37 °C. The formazan crystals were solubilized in Dimethyl Sulfoxide (DMSO, Fisher Scientific, PA, USA) and the absorbance (Abs) was measured at λ = 570 nm and λ = 690 nm (background) on a microplate reader spectrometer (SpectraMax Plus 384 Microplate reader, Molecular Devices, CA, USA).

2.7. Statistical analysis

The results were expressed as means ± standard deviations (SD). The assays were performed in triplicate and, the minimum of three points was assessed on each sample. The statistical tool SigmaStat 3.5 (Systat Software, San Jose, CA, USA) was used for statistical analysis with $p < 0.05$ considered as being statistically significant and $p < 0.01$ considered highly significant. One-Way ANOVA was used to determine the differences between the different groups of surfaces. Tukey HSD post hoc analysis was used for pair-wise comparisons between groups.

3. Results

3.1. Characterization of Ca/P-doped TiO_2 nanotubes

3.1.1. Morphology of TiO_2 nanotubular films

The substrates for nanotube growth were obtained by mechanical polishing of cp-Ti surfaces until mirror finishing (Fig. 1a). The synthesis of nanotubular films comprised of two-step anodization process. Upon first anodization step and ultrasonication, a nano-patterned surface with a concave morphology was formed as shown in Fig. 1b. Afterwards, these nano-imprints were used as the template for the second anodization step, resulting in the formation of NT surfaces characterized by well-defined and well-organized nanotube arrays, as depicted in Fig. 1c. Lower and higher magnification FESEM pictures show the presence of uniformly distributed nanotubes with non-uniform diameters along the surface area. It is also observed that NT surfaces are characterized by the absence of cracks. The morphology of the bottom of the nanotubes is depicted in Fig. 1d. The hexagonal packing density of nanotube arrays shows their high self-ordering level. As described in Section 2.3, NT surfaces were subjected to anodization and reverse polarization treatments in a Ca/P-electrolyte, aiming the incorporation of the bioactive elements into nanotube structure. After these treatments, NT-Ca/P and NT-RP-Ca/P samples were synthesized, and their surface morphology is depicted in Fig. 2a and b, respectively. No differences in morphology were observed. From observation of Figs. 1 c, 2 a and b, it is clear that the morphological features on NT, NT-Ca/P and NT-RP-Ca/P surfaces, are similar. From these figures, diameter and wall-thickness were measured, and the results are depicted in Table 1. NT samples are characterized by nanotubes with an inner diameter of 74.1 ± 13.7 nm and a wall-thickness of 19 ± 4.6 nm. Similar values were found for nanotubes in NT-Ca/P (67.2 ± 13.4 nm diameter, 17.9 ± 3.7 nm wall-thickness) and NT-RP-Ca/P (59.8 ± 12.3 nm diameter, 18.5 ± 3.2 nm wall-thickness) samples.

Nanotubes vertically oriented from Ti substrate were produced, as shown in Fig. 3a. The inset arrow in the figure shows the growing direction of the nanotubes and delimits their length. The FESEM cross sectional images representative of the length of the nanotubular films present on NT, NT-Ca/P and NT-RP-Ca/P samples are depicted in Fig. 3b, c and d, respectively. The average values of the film thickness measured from FESEM images are shown in Table 1. Similar values of thickness were found for nanotubes on NT (12 ± 0.4 μm length) and NT-Ca/P (13 ± 1.6 μm length) samples. On the other hand, as observed in Fig. 3d, the length of the nanotubular film on NT-RP-Ca/P samples was significantly lower, reaching 5.5 ± 0.1 μm (Table 1).

3.1.2. Roughness

Average roughness (R_a) measurements of nanotubular films were extracted from three-dimensional (3D) surface topographies obtained from WLI. The 3D images of Ti, NT, NT-Ca/P and NT-RP-Ca/P samples are shown in Fig. 4 and the correspondent R_a values

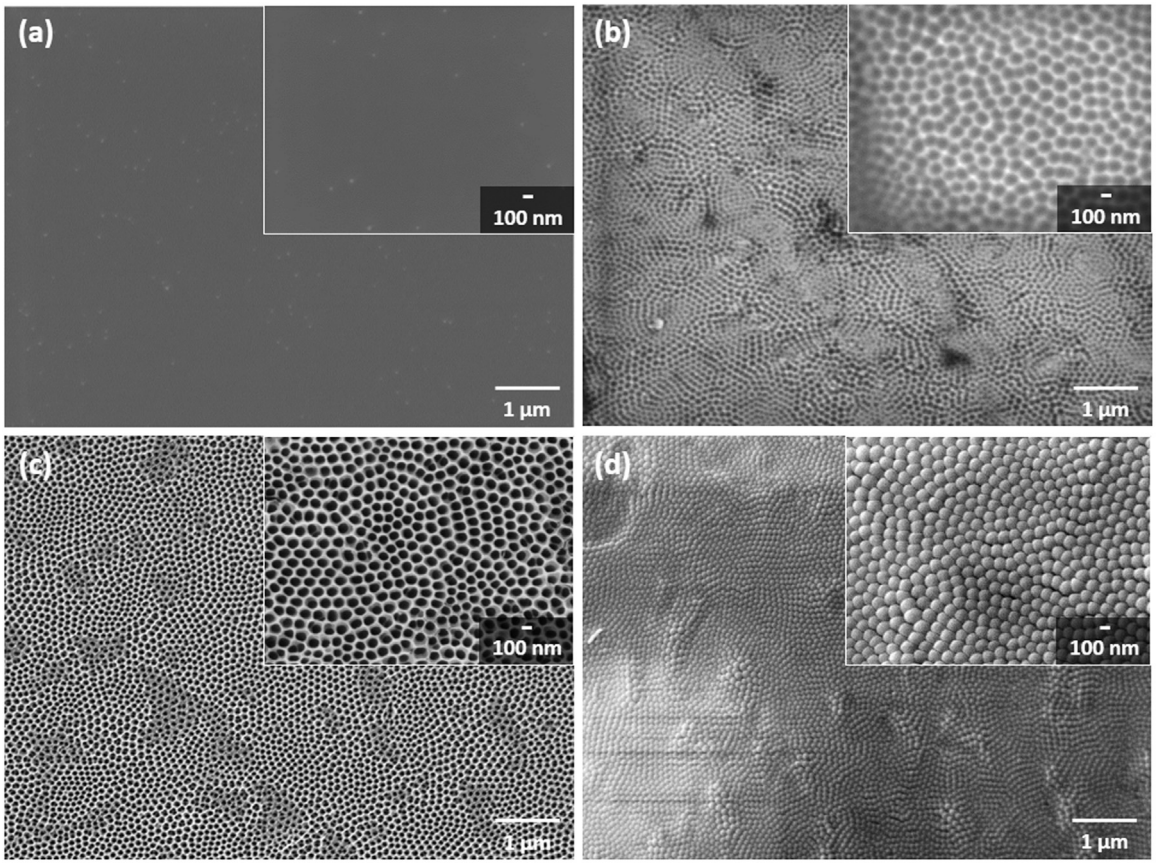

Fig. 1. FESEM micrographs of (a) Ti smooth and (b) nanopatterned Ti surfaces as a consequence of nanotube detachment after the first anodizing step. In (c) the FESEM image of well ordered TiO_2 nanotubes synthesized after the second anodizing step (NT surface) is shown, and finally, (d) the bottom morphology of the highly ordered nanotube arrays present on NT surfaces is observed. Higher magnification pictures are shown in the right upper corner of individual pictures.

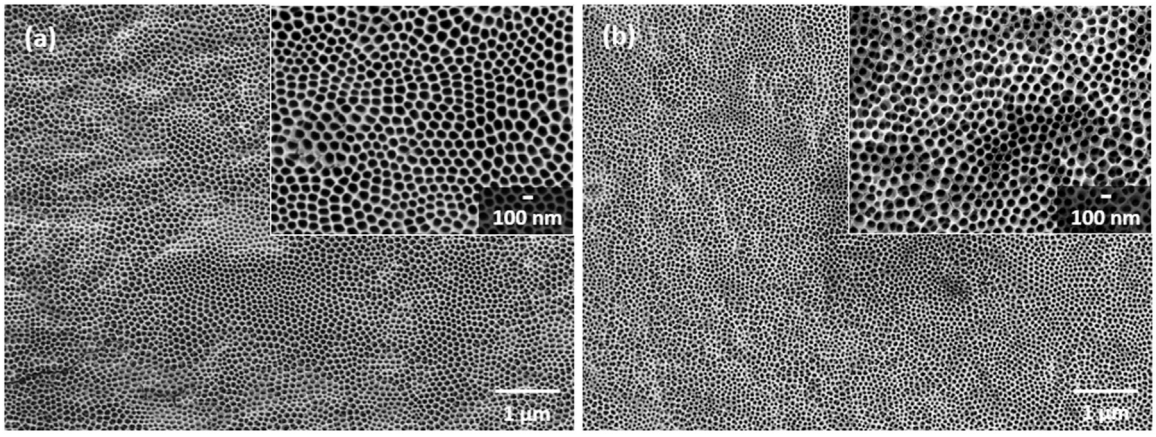

Fig. 2. FESEM micrographs showing the morphology of the highly ordered TiO_2 nanotubes present on (a) NT-Ca/P and (b) NT-RP-Ca/P surfaces. Higher magnification pictures are shown in the right upper corner of individual pictures.

depicted in Table 2. It is clear from 3D images depicted in Figs. 4a and b that the surface topography of Ti is significantly different from NT surface as a result of the growth of a micron-length nanotubular film on Ti. These differences are reflected in the significant increase of the R_a values from 0.05 ± 0.01 µm to 7.40 ± 0.13 µm (Table 2). The 3D image of NT-Ca/P (Fig. 4c) as well its R_a value of 7.33 ± 0.47 µm (Table 2), show that they present similar topographical features to NT surfaces. On the other hand, the 3D image representative of NT-RP-Ca/P surfaces (Fig. 4d) shows that the reverse polarization step induced to a different film topography

Table 2
Average roughness (R_a) of Ti, NT, NT-Ca/P and NT-RP-Ca/P surfaces measured by WLI.

Group	Average roughness (R_a) (µm ± SD)
Ti	0.05 ± 0.01
NT	$7.40 \pm 0.13^{*}$
NT-Ca/P	$7.33 \pm 0.47^{*}$
NT-RP-Ca/P	$5.67 \pm 0.10^{*\#}$

(*) significantly different from Ti; (#) significantly different from NT and NT-Ca/P; $p < 0.001$.

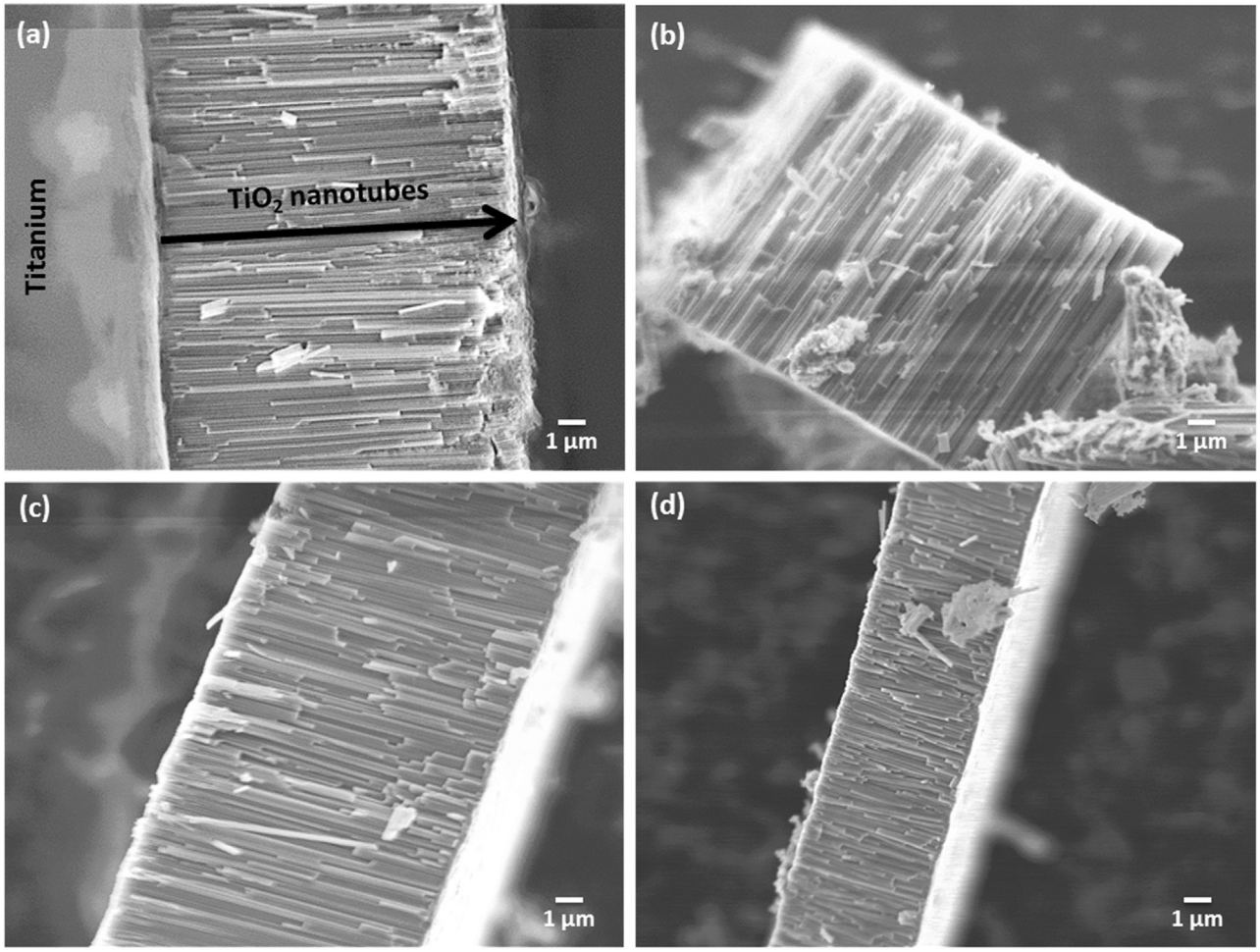

Fig. 3. Cross sectional FESEM image representative of TiO_2 nanotubes grown vertically oriented from Ti substrate. The inset indicates the growing direction of the nanotubes and delimits their length. The length of the nanotubes is observed by FESEM images for (b) NT, (c) NT-Ca/P and (d) NT-RP-Ca/P samples.

characterized by a significant lower R_a value ($5.67 \pm 0.10\,\mu m$). In general, a high surface uniformity of the nano-arrays grown from Ti was noticed.

3.1.3. Chemical composition

The EDS spectra acquired from Ti and NT surfaces are shown in Fig. 5a and b, respectively. It is observed that after two-step anodization process, Oxygen (O) and Fluorine (F) were present on NT surfaces, beyond Ti and Carbon (C), elements that were also detected on Ti substrate. From EDS spectra of NT-Ca/P and NT-RP-Ca/P shown respectively in Fig. 5c and d, Ca and P elements were also detected in addition to the previously detected elements.

The binding states of the chemical elements detected on nanotubular surfaces were studied by XPS. Chemical elements such as C 1s, Ti 2p, O 1s and F 1s were detected on NT surfaces and the presence of Ca 2p and P 2p was confirmed on NT-Ca/P and NT-RP-Ca/P surfaces. Aiming to study the binding states of the detected elements, their individual spectra were deconvoluted into their components. C 1s peak at 284.6 eV was used as a reference binding energy for calibration [45] and a nonlinear (Shirley) background correction method was used for electron backgroung correction, which is the most commonly accepted and widely used [46]. The XPS individual spectra of the detected elements on NT, NT-Ca/P and NT-RP-Ca/P surfaces are shown in Fig. 6, Fig. 7 and Fig. 8, respectively. The deconvoluted peaks are shown in the individual spectra of the detected elements as well as the information obtained from deconvolution with reference to the subpeak binding energy and the possible chemical compound assigned to it, atomic percentage (at.%) and also to the chi square values (χ^2) associated to the deconvolution of each spectrum.

The presence of C—C and C—O groups and also organic C 1s was detected on all the nanotubular surfaces at similar binding energies, as shown in Figs. 6–8. TiO_2 and Ti_2O_3 were present on all the surfaces, with a significantly higher at.% detected for TiO_2. Besides, the presence of F ions adsorbed to TiO_2 nanotubes was found on all the groups. After functionalization processes through anodization of NT surfaces in the Ca/P-electrolyte, these were characterized also by the presence of CaF_2 and $CaCO_3$ compounds. Furthermore, $Ca_3(PO_4)_2$ and/or $CaHPO_4$ compounds were also found on NT-Ca/P and NT-RP-Ca/P surfaces. Interestingly, CaO appeared only on NT-RP-Ca/P surfaces, which means, when NT surfaces were submitted to reverse polarization process for 10s, immediately before anodization in the Ca/P-electrolyte.

The FTIR spectra of NT, NT-Ca/P and NT-RP-Ca/P surfaces are shown in Fig. 9. In all FTIR spectra H_2O ($\sim$3600–3800 cm^{-1}) and gas phase carbon dioxide (CO_2) absorption bands ($\sim$2200–2400 cm^{-1}) were detected, which resulted due to the residual air in the FTIR purging chamber [47–49]. Furthermore, the absorption band from $\sim$3000–3500 cm^{-1}, is possibly attributed to fundamental stretching vibration of H_2O and OH groups [50–56]. The presence of CH_2 stretching modes was noticed at 2937.2 cm^{-1} and 2870.5 cm^{-1} for NT, NT-Ca/P and NT-RP-Ca/P surfaces. The region comprised between 1200 and 1900 cm^{-1} consists of the superposition of various absorption bands. The absorption peaks at this region can be

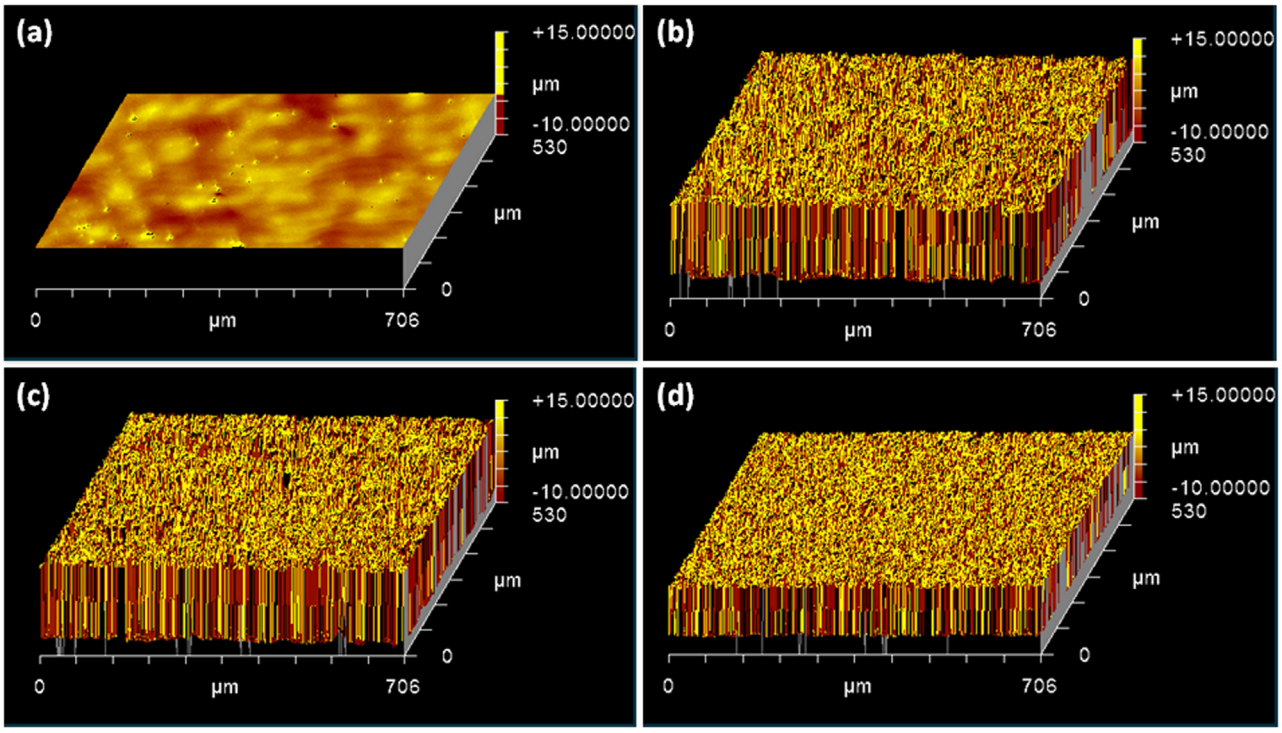

Fig. 4. Tridimensional topographies of (a) Ti, (b) NT, (d) NT-Ca/P and (e) NT-RP-Ca/P samples obtained from WLI measurements.

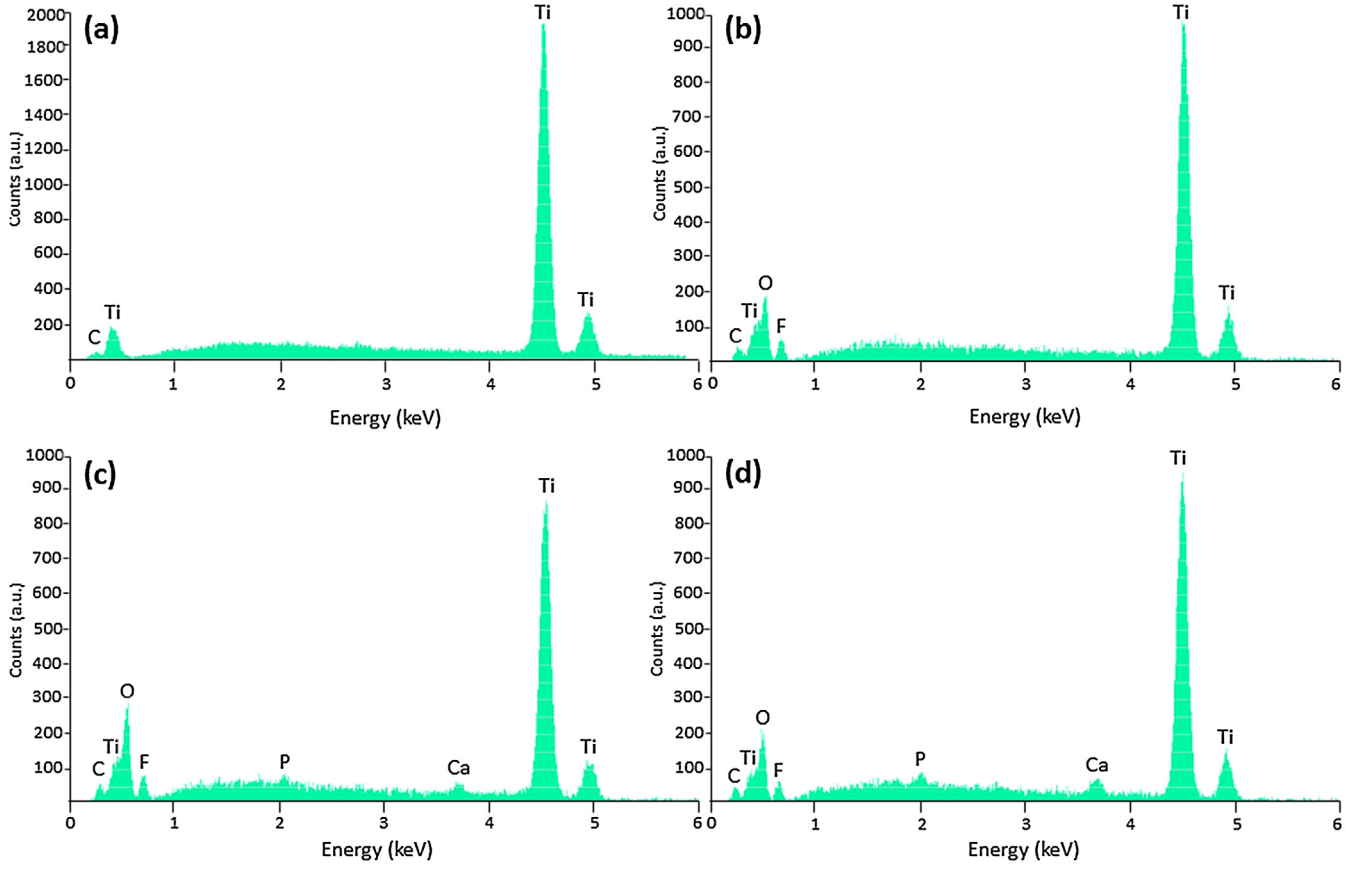

Fig. 5. EDS spectra of (a) Ti, (b) NT, (d) NT-Ca/P and (e) NT-RP-Ca/P samples.

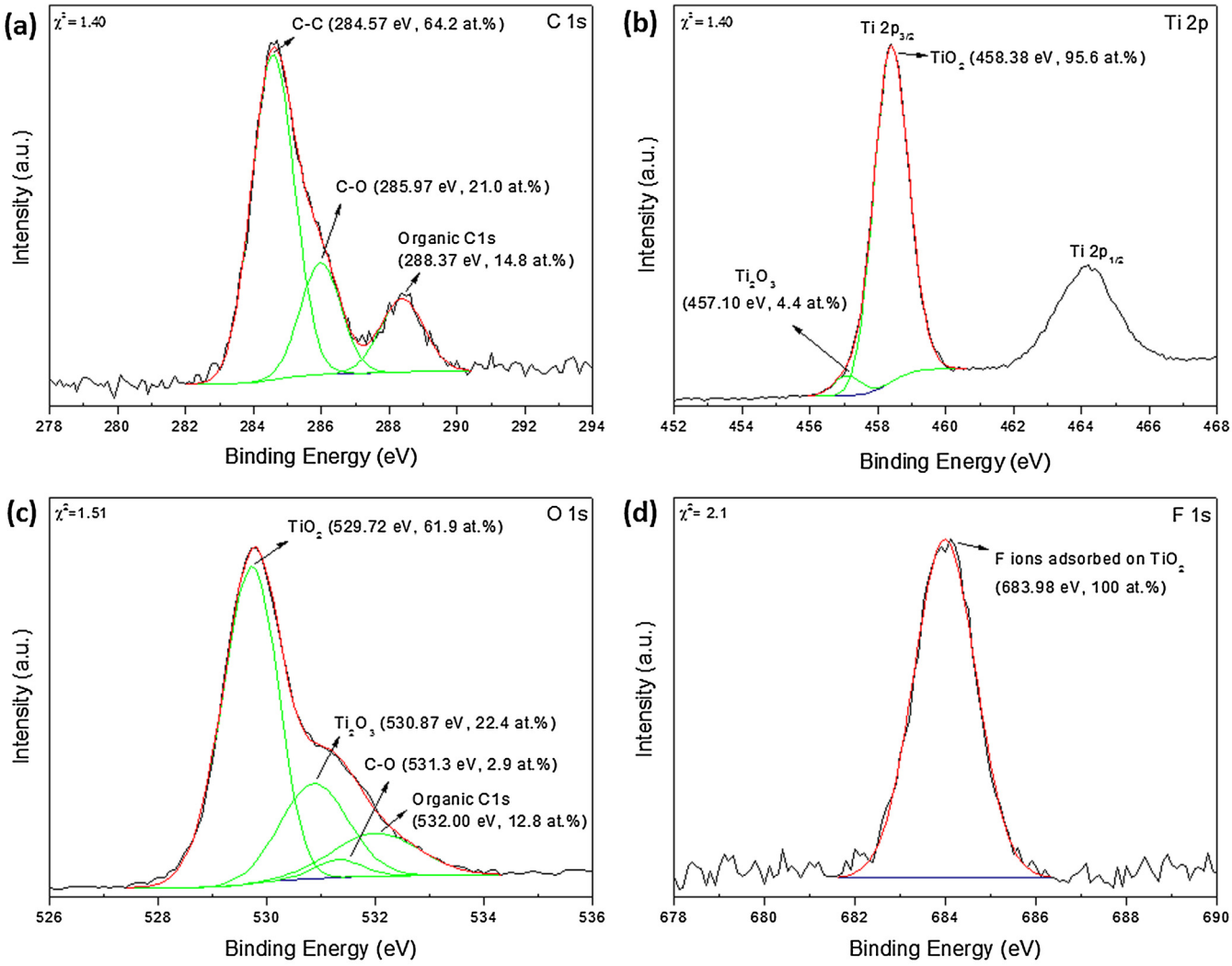

Fig. 6. High resolution XPS spectra of deconvoluted (a) C 1s, (b) Ti 2p, (c) O 1s and (d) F 1s elements detected on NT surface. The information obtained from deconvolution is shown in each individual spectrum with reference to the subpeak binding energy and the possible chemical compound assigned to it, atomic percentage (at.%) and also to the chi square values ($\chi 2$) associated to the deconvolution of the spectrum.

assigned to the bond stretch of NH_4^+ and adsorbed NH_3 on TiO_2 from the electrolyte [47]. Moreover, IR bands in the spectral range of 1300–1700 cm^{-1} may be an indicator of the presence of molecularly adsorbed O_2, CO_2, and CO molecules on TiO_2 [50]. The region between ~600–1200 cm^{-1} is also characterized by the superimposition of different absorption bands. According to different studies, this region is generally assigned to the presence of Ti—O, Ti—OH and TiO_2 [46,47,49]. Absorption peaks at 1018.5 cm^{-1} and 1086.4 cm^{-1} can be assigned to the presence of PO_4^{3-} groups on NT-Ca/P and NT-RP-Ca/P surfaces [57]. The absorption band at 1030.9 cm^{-1} may be related either to the presence of Ti—OH vibrations and PO_4^{3-} groups [47,58,59]. Finally, the presence of PO_4^{3-} groups can also be assigned to the absorption peak that appears at 972.2 cm^{-1} [58].

3.1.4. Wettability

The wettability of Ti and nanotubular surfaces was investigated by WCA measurements, and the results are depicted in Table 3. The WCA measured for polished Ti was of 45 ± 3.1°, indicating that this surface is hydrophilic (WCA < 90°) [60]. After anodization of Ti, the hydrophilicity of the surface was enhanced as shown by the significant decrease in the WCA measured for NT surfaces to 14.3 ± 2.2° ($p < 0.001$). The WCA measured for NT-Ca/P and NT-RP-Ca/P surfaces were 11.8 ± 2.8° and 10.5 ± 3.0°, respectively. These values are similar to the ones measured on NT surfaces and significantly lower than WCA of Ti ($p < 0.001$).

Table 3
WCA measured on Ti, NT, NT-Ca/P and NT-RP-Ca/P surfaces.

Group	WCA (° ± SD)
Ti	45.4 ± 3.1
NT	14.3 ± 2.2*
NT-Ca/P	11.8 ± 2.8*
NT-RP-Ca/P	10.5 ± 3.0*

(*) significantly different from Ti; $p < 0.001$.

3.2. Electrochemical studies

The potentiodynamic polarization curves of Ti, NT, NT-Ca/P and NT-RP-Ca/P surfaces are depicted in Fig. 10 and the current values extracted from the passivation region of these curves (I_{pass}), are listed in Table 4. The nanotubular surfaces exhibit a passive region extended over a wide potential range and display a fast and effective passivation behavior as compared to Ti, which is probably related to the effective blockage of the current provided by

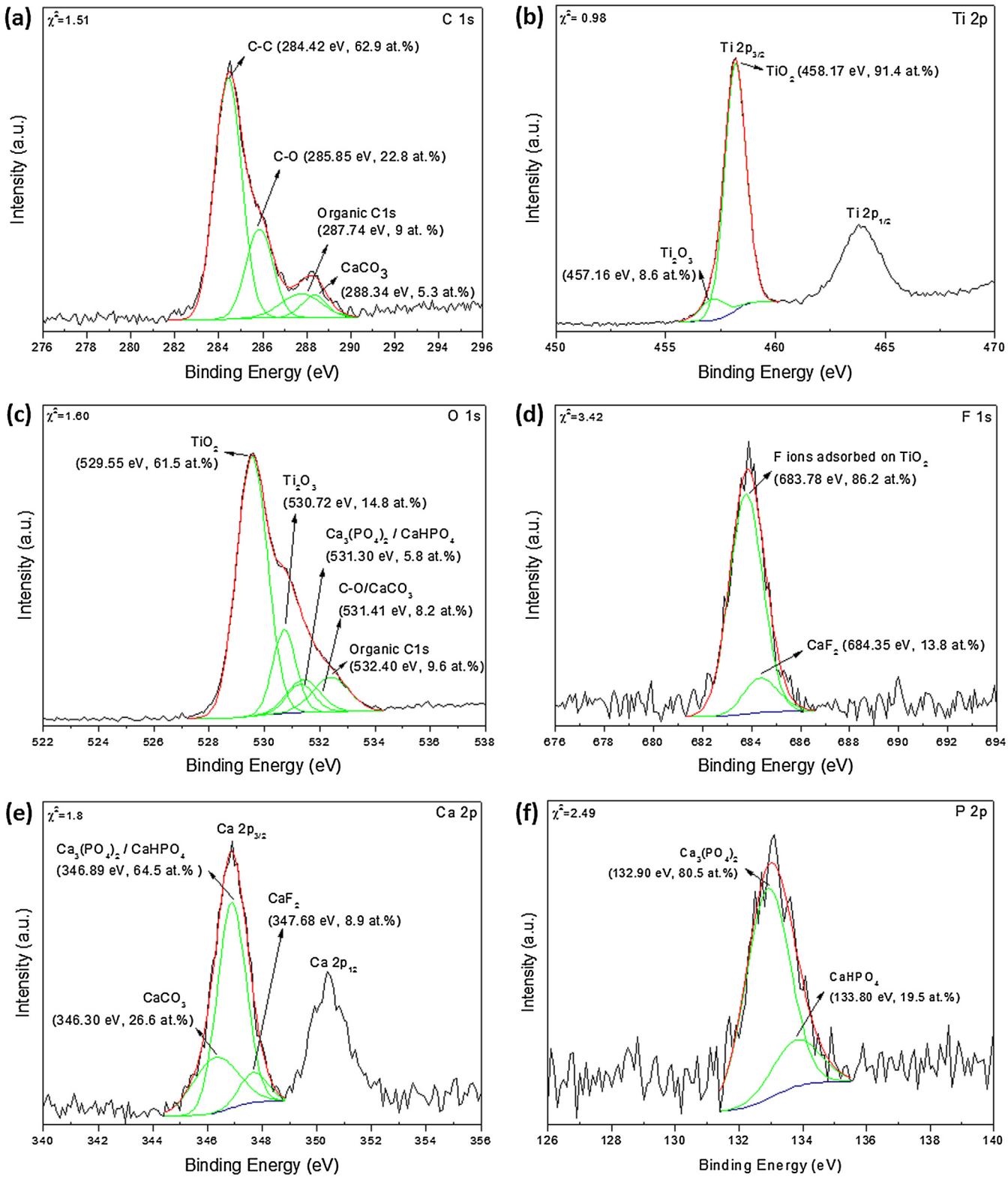

Fig. 7. High resolution XPS spectra of deconvoluted (a) C 1s, (b) Ti 2p, (c) O 1s, (d) F 1s, (e) Ca 2p and (f) P 2p elements detected on NT-Ca/P surface. The information obtained from deconvolution is shown in each individual spectrum with reference to the subpeak binding energy and the possible chemical compound assigned to it, atomic percentage (at.%) and also to the chi square values ($\chi 2$) associated to the deconvolution of the spectrum.

nanotubular films properties. The I_{pass} was similar for Ti and NT surfaces, however, NT-Ca/P and NT-RP-Ca/P surfaces revealed significantly lower I_{pass} values (Table 4), suggesting a higher corrosion resistance property [61].

3.3. *Biological characterization of Ca/P-doped TiO_2 nanotubes*

3.3.1. *Morphology of MG-63 cells*

MG-63 cells adhered on Ti, NT, NT-Ca/P and NT-RP-Ca/P surfaces were imaged by FESEM aiming to access their morphology as

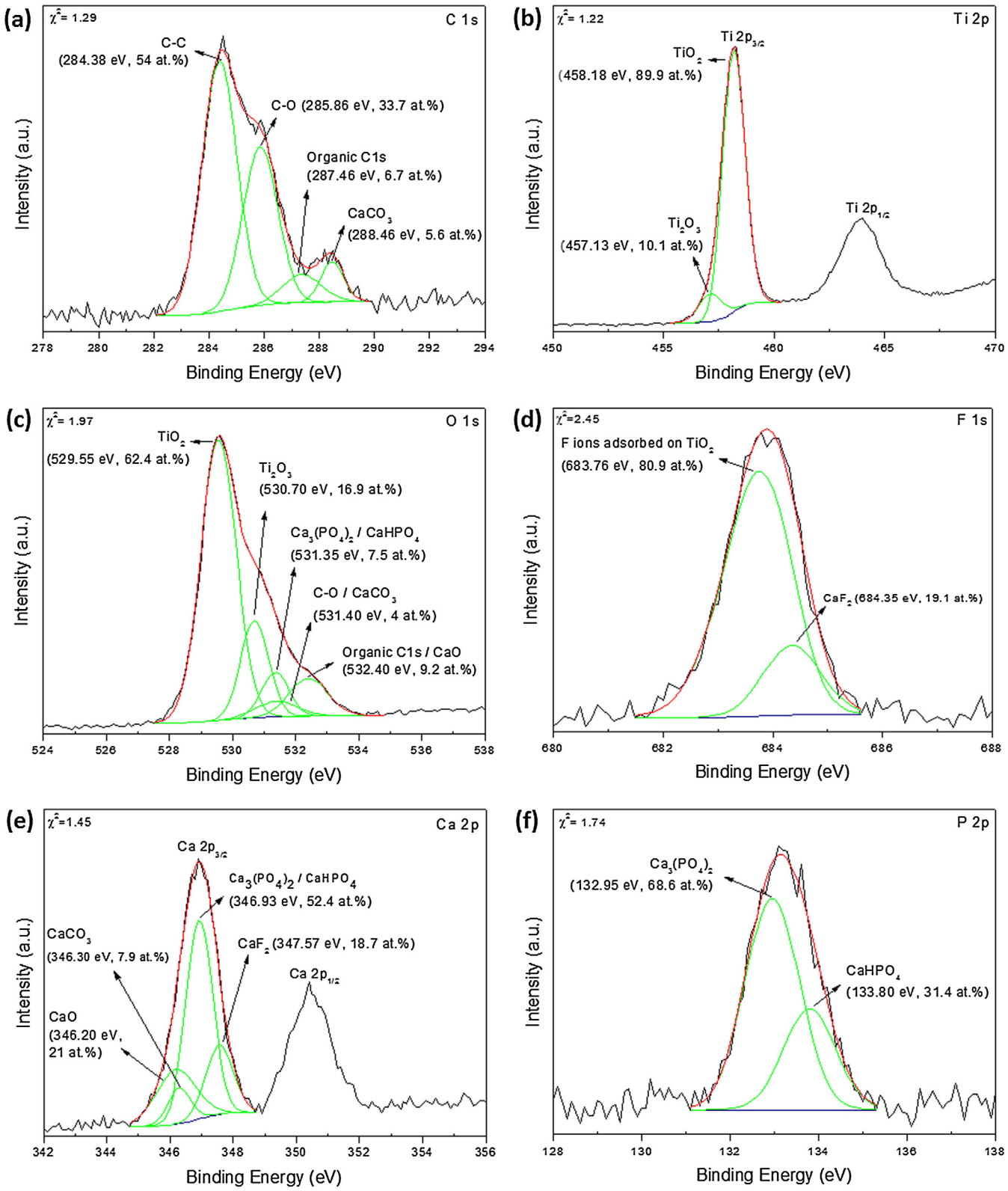

Fig. 8. High resolution XPS spectra of deconvoluted (a) C 1s, (b) Ti 2p, (c) O 1s, (d) F 1s, (e) Ca 2p and (f) P 2p elements detected on NT-RP-Ca/P surface. The information obtained from deconvolution is shown in each individual spectrum with reference to the subpeak binding energy and the possible chemical compound assigned to it, atomic percentage (at.%) and also to the chi square values ($\chi 2$) associated to the deconvolution of the spectrum.

well as their interaction with materials surface. In Fig. 11 the correspondent FESEM micrographs are shown, after one and six days of incubation. As observed in Fig. 11 (a1, b1, c1 and d1) cells adhere on the materials surface after one day of incubation, presenting different morphologies. Cells adhered on Ti surfaces (Fig. 11 a1) seem less spread than the ones adhered on nanotubular surfaces (Fig. 11 b1, c1 and d1). The cells on nanotubular surfaces present a spreader morphology, and they are interconnected. It should be

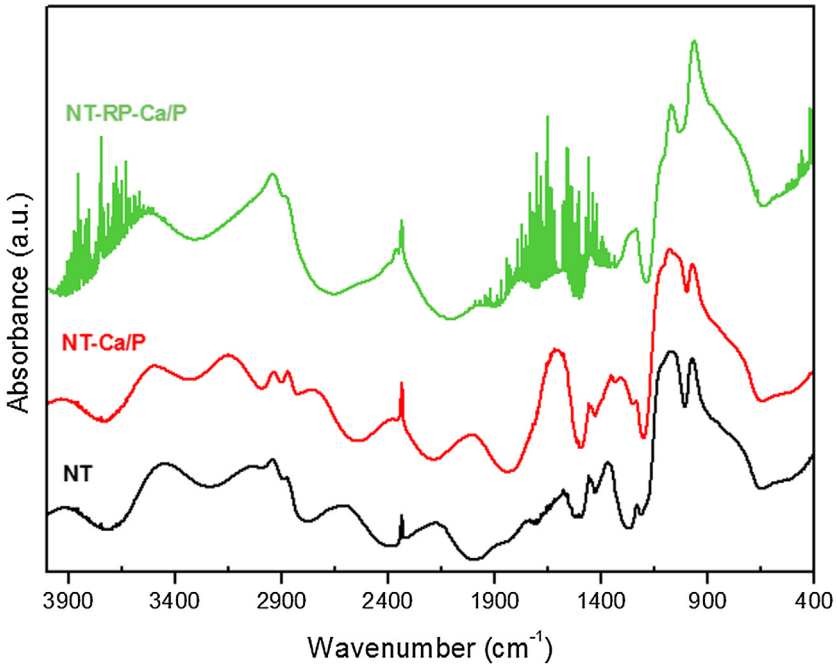

Fig. 9. FTIR spectra of NT, NT-Ca/P, and NT-RP-Ca/P surfaces. The different groups of surfaces are properly identified in the figure.

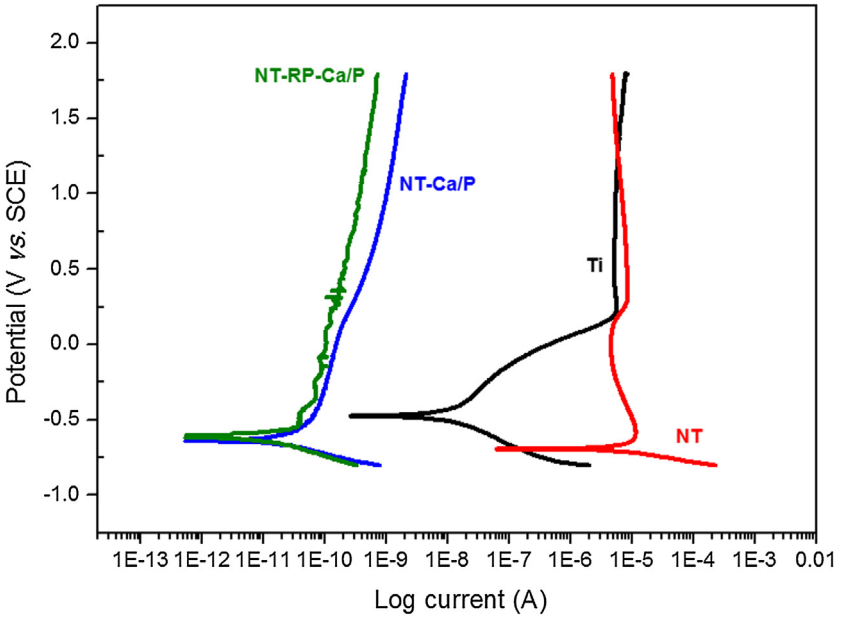

Fig. 10. Potentiodynamic polarization curves of Ti, NT, NT-Ca/P and NT-RP-Ca/P samples immersed in AS at 37 °C. Surface area exposed to AS: 0.4 cm^2; potential scan rate: 2 mV s^{-1}; potential scan from −0.8 to + 1.8 V *vs.* SCE. The different groups of samples are properly identified in the figure.

Table 4
Passive current (I_{pass}) values measured from potentiodynamic polarization curves of Ti, NT, NT-Ca/P and NT-RP-Ca/P samples immersed in AS at 37 °C.

Group	I_{pass} (A)
Ti	$5.47 \times 10^{-6} \pm 1.79 \times 10^{-7}$
NT	$6.86 \times 10^{-6} \pm 1.59 \times 10^{-6}$
NT-Ca/P	$2.88 \times 10^{-10} \pm 3.59 \times 10^{-11}$*
NT-RP-Ca/P	$1.10 \times 10^{-9} \pm 4.40 \times 10^{-7}$*

(*) significantly different from Ti and NT; $p < 0.001$.

noticed that at this time point, the osteoblastic cells adhered on materials surface present filopodia forming adhesion points at the surface and establishing cell–cell contact as demonstrated by the inserts included in higher magnification FESEM micrographs. After six days of incubation, there is an increased number of adhered cells as observed on each different group in Fig. 11 (a2, b2, c2 and d2). At day six the materials surface is covered by an abundant cell layer, and all the cells seem well spread and interconnected.

Fluorescence microscopy images of MG-63 cells adhered on Ti, NT, NT-Ca/P and NT-RP-Ca/P surfaces, after one and six days of incubation, are depicted in Fig. 12. After one day of culture (Fig. 12 a1, b1, c1 and d1), the cells already adhered on materials surface, and a similar number of cells seems to be present on all the groups. At this time point, adhered cells present spherical, spread and elongated morphologies. In general, cell-to-cell contact is observed to a large

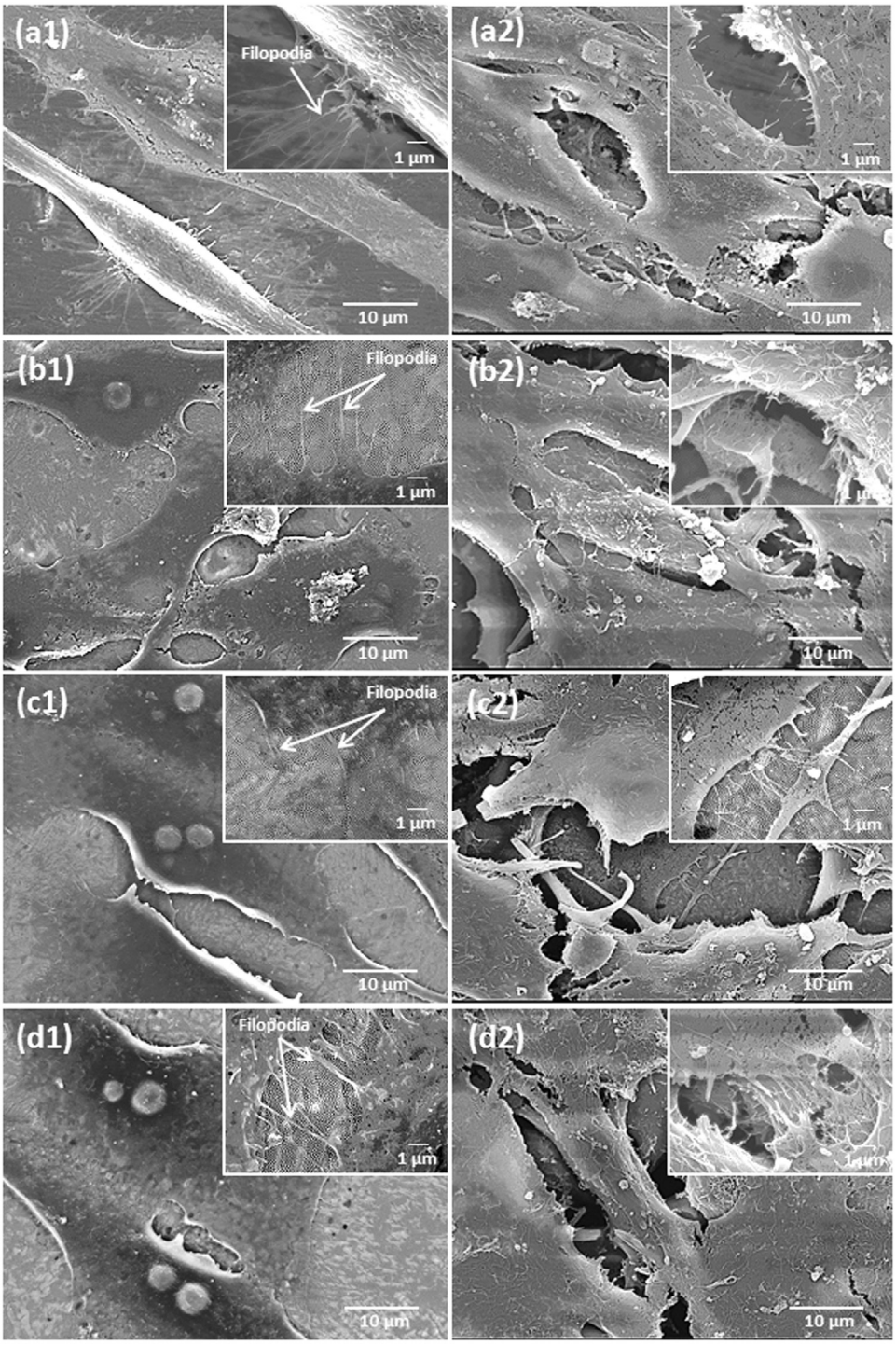

Fig. 11. FESEM micrographs of MG-63 cells cultured on Ti, NT, NT-Ca/P and NT-RP-Ca/P surfaces after one and six days of incubation: MG-63 cells on (a1) Ti, (b1) NT, (c1) NT-Ca/P and (d1) NT-RP-Ca/P surfaces – day one; MG-63 cells on (a2) Ti, (b2) NT, (c2) NT-Ca/P and (d2) NT-RP-Ca/P surfaces – day six.

extent. After six days of culture, there is an increase in the number of the adhered cells except for NT-Ca/P surfaces as shown in Fig. 11 (a2, b2, c2 and d2). In Fig. 11 c2 it is observed that MG-63 cells are more scarcely distributed presenting a less spread morphology along NT-Ca/P surfaces as compared to the other groups.

3.3.2. Metabolic activity of MG-63 cells

The metabolic activity of MG-63 cells seeded on Ti, NT, NT-Ca/P and NT-RP-Ca/P surfaces was investigated by MTT reduction assay after one and six days of incubation and the correspondent absorbance values are shown in Fig. 13. Once MTT reduction is attributed to mitochondrial succinate dehydrogenase redox activity, the absorbance values are proportional to cell metabolism, and

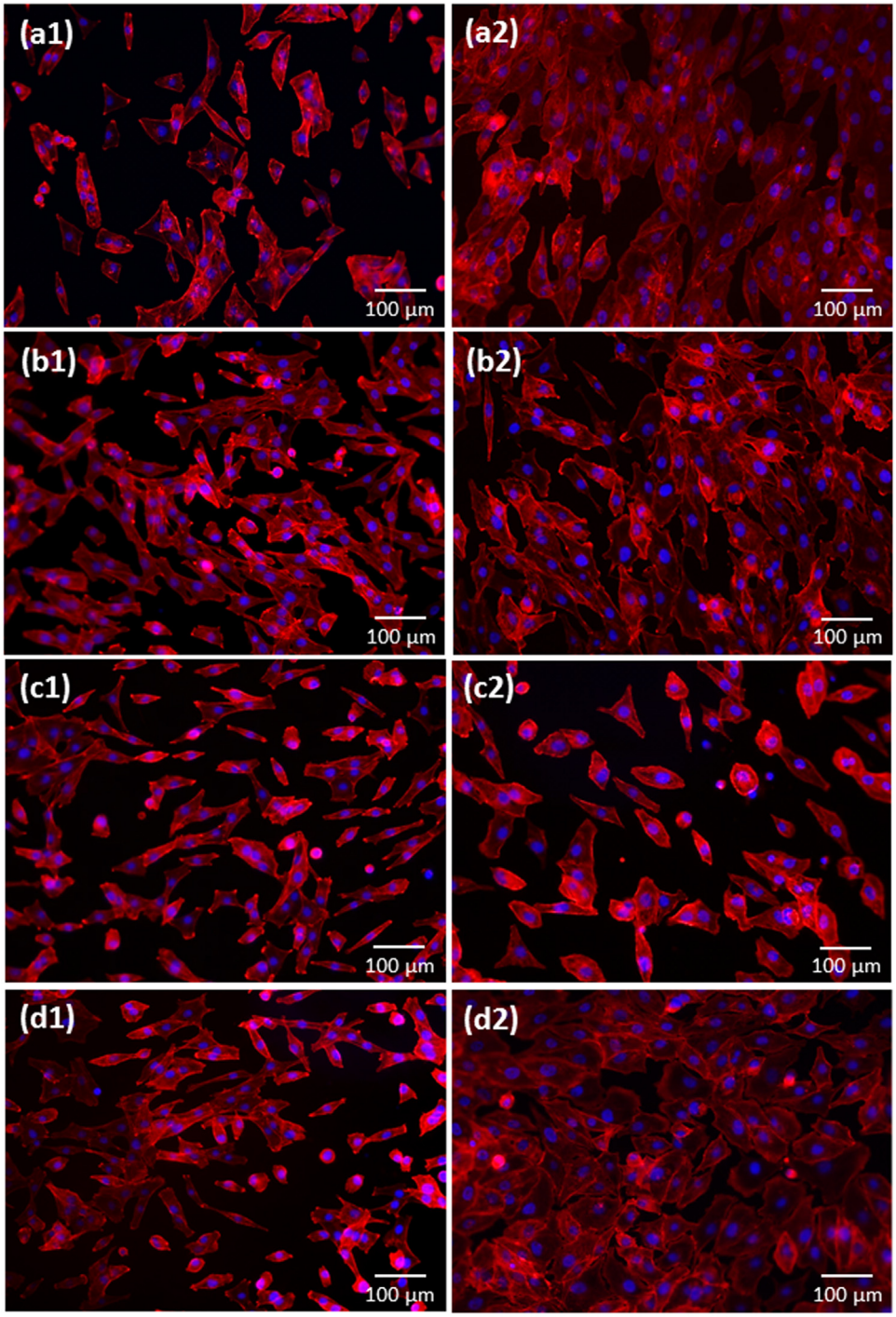

Fig. 12. Fluorescence microscopy images of MG-63 cells cultured on Ti, NT, NT-Ca/P and NT-RP-Ca/P surfaces after one and six days of incubation: MG-63 cells on (a1) Ti, (b1) NT, (c1) NT-Ca/P and (d1) NT-RP-Ca/P surfaces – day one; MG-63 cells on (a2) Ti, (b2) NT, (c2) NT-Ca/P and (d2) NT-RP-Ca/P surfaces – day six.

therefore, cell viability. Additionally, an increase in cell viability is an indicator of cell proliferation [11,62].

At day one of culture, MG-63 cells present a similar metabolic activity level as shown by the similar absorbance values depicted for all the groups (Fig. 13). At day six, the absorbance values significantly increased for all the materials, suggesting that the metabolic activity increased and that cells proliferated with time. However, remarkable differences are observed between the different groups. At this time point, the cells cultured on NT-RP-Ca/P present significantly higher metabolic activity than NT-Ca/P and Ti, and similar to NT surfaces.

4. Discussion

4.1. Morphological and topographical features of Ca/P-doped TiO_2 nanotubes

It is commonly accepted that the mechanism for nanotube formation by anodization in a fluoride-containing electrolyte is based on a field-assisted dissolution process consisting of two main stages: 1) the anodic oxidation of Ti metal to form a passive Ti oxide film on its surface by the recombination of Ti^{4+}, O^{2-} and OH^{-} ions, moving under the action of an electric field and, 2) the

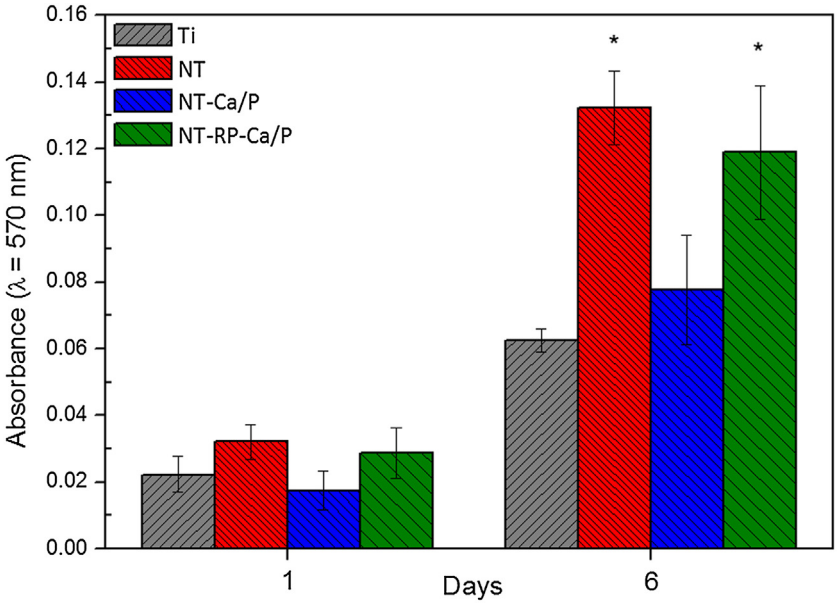

Fig. 13. Metabolic activity of MG-63 cells cultured on Ti, NT, NT-Ca/P and NT-RP-Ca/P surfaces after one and six days of incubation. At day six: (*), significantly different from Ti and NT-Ca/P; $p < 0.05$.

local chemical dissolution of the growing oxide by fluoride ions (F^-) and pore formation [26,63–65]. This process assumes that the growth of nanotubes is ensured by the balance between the formation of an oxide barrier film at the metal-oxide interface and, the field-enhanced dissolution at the base of the pores/tubes, where the electric field is stronger [65].

It is already documented in literature that the self-ordering of TiO_2 nanotubes is improved after multi-step anodic oxidation processes [66]. As stated by Serikov et al. [67] the repeated anodization of titanium, is one way of structuring the surface, removing contaminants and increasing the adhesion of the synthesized nanotubes. Based on this knowledge, in this study, nanotubular structures were synthesized using a two-step anodization process. Firstly, the nanotubes were produced by anodization of Ti polished surfaces (Fig. 1a). After this step, the nanotube layer grown from Ti was intentionally ultrasonically peeled off aiming at the formation of a nano-patterned surface presenting concave dimples (Fig. 1b), the common shape of the nanotube bottom [66]. These hemispheric nano-imprints were used as the template for the second anodizing step, once they acted as nucleation sites for the initial pore formation [68,69] required for the growth of highly ordered nanotube arrays. The surface produced after the second anodizing step was named as NT and it is characterized by well-defined and well-organized nanotubes as shown in lower and higher magnification FESEM pictures in Fig. 1c. On the NT surface the absence of cracks and the presence of uniformly distributed nanotubes with non-uniform diameters along the surface area are noticed.

From nanotube bottom morphology depicted in Fig. 1d the hexagonal packing density of nanotube arrays is clearly appearing, which allows the evaluation of the self-ordering of the nanotubular film produced. Han et al. [66] synthesized well-ordered TiO_2 nanotubes by a multi-step anodic oxidation process carried out at 50 V for 5 h, in EG electrolyte containing 0.25 wt.% NH_4F. The authors concluded that the hexagonal packing density of the TiO_2 nanotubes was significantly improved after the multi-step anodic oxidation. These authors also reported that the area densities of the hexagonal TiO_2 arrays increased approximately three times from the first to the second anodic oxidation step. According to Sulka et al. [70] in an ideally arranged triangular lattice, each pore should be surrounded by six neighboring pores. When looking at Fig. 1d, it is observed that nanotube arrays with hexagonally packed arrangement are present over a large surface area. From the above discussed results, the morphological features of the nanotubes are highly dependent on the morphology of the nano-patterned substrates from where they were grown.

The morphological and surface topographical features of osseointegrated implants play a significant role on the mechanical stability of the implant once allocated into bone as well as on the healing and osseointegration processes. In the natural bone tissue, a non-uniform porosity due to the existence of cortical (3–12% porosity, pore sizes: 10–500 μm) and trabecular bones (50–90% porosity, pore sizes: 0.2–1 mm) is noticed. Interestingly, NT surfaces are also characterized by non-uniform pore diameters, varying at a nano-scale level and presenting a very similar morphology when compared to the structure of natural bone. Considering that natural bone is a nanostructured material [71] and bone tissue response is mainly dictated by processes controlled at the nanoscale level [34], it is hypothesized that mimicking the microstructure of bone at a nano-scale level is an interesting approach for the development of a novel surface able to improve the performance of osseointegrated implants. Furthermore, in the attempt to develop a new strategy for obtaining biomimetic systems mimicking the natural extracellular microenvironments, the functionalization of TiO_2 nanotubes with elements natively present in natural bone, namely, Ca and P, was carried out using anodization of NT surfaces in an electrolyte composed of CaA and β-GP (Ca/P-electrolyte). Using this process, the incorporation of bioactive elements present in the anodizing solution into nanotube structure was aimed. As described in Section 2.3, a cathodic polarization step was also applied to NT samples, right before the anodizing process in the Ca/P-electrolyte. With this the cathodic polarization step, it was intended to direct Ca^{2+} ions to NT surface for further incorporation of these elements into nanotube structure. After the anodizing processes carried out in both conditions, NT-Ca/P and NT-RP-Ca/P samples were synthesized, and their surface morphologies are depicted in Fig. 2a and b, respectively. Well-ordered and opened nanotubes, cleared of any aggregations are observed in both cases. From observation of Figs. 1 c and 2, it is clear that NT, NT-Ca/P and NT-RP-Ca/P samples display similar morphological features, as confirmed by diameter and wall thickness measurements reported in Table 1. The novelty of this method and

what distinguishes it from other bio-functionalization processes commonly reported in literature [10,35], lies on the usage of NT samples as the cathode and, immediately after, as the anode, in the electrochemical cell.

It has been reported that cell fate is determined by the TiO_2 nanotube sizes in vitro, but optimum scale is still controversial. Wang et al. [6] reported that a significant increase in bone implant contact and gene expression levels was found in the bone attached to TiO_2 nanotubes, especially with 70 nm diameter. On the other hand, Park et al. [4] demonstrated that adhesion, proliferation, migration and differentiation of MSCs was maximally induced on 15 nm nanotubes, but prevented on 100 nm. In our study, non-uniform pore diameter ranging at a nano-scale level between 45 and 90 nm were formed, with potential to improve cell-materials interactions.

The representative picture of the nanotubes grown vertically oriented from the Ti substrate is shown in Fig. 3a. As observed from cross sectional images representative of the length of NT and NT-Ca/P nanotubular films (Fig. 3b and c, respectively), and from the correspondent values in Table 1, nanotubes with similar thickness were formed. These results indicate that the second anodizing process did not influence the length of the nanotubular film present on NT surfaces. On the other hand, the length of NT-RP-Ca/P nanotubes was significantly lower (Fig. 3d) what might be attributed to the reverse polarization step applied on the NT samples during 10 s in the Ca/P-electrolyte. For reverse polarization step, the polarity of the electrodes was inverted. By this way, NT samples became the cathode and the graphite rod, the anode. According to Abellán et al. [72], the passive titanium oxide film might undergo different processes when submitted to cathodic polarization: various stages of oxide reduction up to oxide dissolution, the adsorption and absorption of hydrogen, hydrogen evolution, and oxygen reduction. It has been reported that when a titanium electrode covered with TiO_2 film is polarized in the potential range where hydrogen evolution reaction takes place, a decrease in film thickness occurs. This phenomenon is produced by the partial reduction of the Ti^{4+} present in TiO_2 film to Ti^{3+} in oxy-hydroxi species [73]. The cathodic potential of −0.6 V *vs. SCE* is considered as the potential that can render the protective oxide ineffective as a barrier by reducing it from TiO_2 to TiOOH. In the present work the cathodic cell potential of 20 V was applied to NT samples for 10 s. After this process, there was a significant decrease in the thickness of the nanotubular film. It is believed that the reactions which cause the thinning phenomenon of the film involved a high level of chemical dissolution of the TiO_2 nanotubular film due to the high cathodic potential applied during the process. Most probably, the dissolution occurred due to the reduction of TiO_2 nanotubes into oxy-hydroxi species [73,74], which may be dissolved in the electrolyte or precipitate at the top of the film [73].

The average roughness (R_a) of nanotubular films was extracted from three-dimensional (3D) surface topographies obtained from WLI. A high level of uniformity of the nano-arrays growth from Ti is noticed from the 3D images (Fig. 4). These images reflect the phenomenon of film thinning by reverse polarization step. The significantly lower thickness of nanotubes is reflected on 3D image of NT-RP-Ca/P sample (Fig. 4d) and also on the correspondent R_a value (Table 2), which is significantly lower than the ones measured for NT and NT-Ca/P surfaces.

4.2. Chemical and physico-chemical features

After the two step anodization process, Ti, O, and F were detected on NT surfaces by EDS (Fig. 5b) and XPS (Fig. 6). The existence of these elements on NT surfaces is related to growth of an oxide film via anodization of Ti in a F-containing electrolyte. During anodization of Ti, its oxidation takes place with release of Ti^{4+} ions and electrons. The anodic potential applied during the process controls the rate of ion migration within the metal/electrolyte interface. The Ti^{4+} ions can be consumed for the film development by their recombination with OH^- and O^{2-} species provided by the field-assisted water dissociation, and/or field-assisted driven from the Ti substrate towards the electrolyte [65,75]. This can result in the formation of oxide (i.e. TiO_2) or hydrated oxide (i.e. $Ti(OH)_4$). The fluorine ions present in the electrolyte can chemically dissolve both the hydrated and oxide layers, or react with Ti^{4+} ions [65,75]. For NT-Ca/P and NT-RP-Ca/P surfaces, Ca and P elements were also detected by EDS (Fig. 5c and d) and XPS (Figs. 7 and 8). This shows that after anodization processes carried out in the Ca/P-electrolyte, bioactive elements were successfully incorporated in nanotubular surfaces.

To investigate the chemical compounds possibly assigned to the detected elements, the individual XPS spectrum of each element was resolved into their components by curve fitting.

Fig. 6a shows the deconvolution of C 1s main peak on NT surface into three subpeaks characterizing the chemical states of carbon. The sub-peak at 284.57 eV is generally assigned to the presence of adventitious carbon [76–78] inevitable adsorbed from the atmosphere while the C 1s subpeaks at 285.97 eV and 288.37 eV may be related to C—O bonds and organic C 1s, respectively [78–80]. Carbon was also detected on TiO_2 nanotube arrays synthesized by Han et al. [66] at similar anodizing conditions of the present study. The authors explained that carbon was associated to species such as hydrocarbon (C—H), hydroxyl (C—OH) and carboxyl (O=C—OH) groups. This is in good agreement with FTIR results with IR bands in the spectral range of 1300–1700 cm^{-1} as an indicator of the presence of molecularly adsorbed CO groups on TiO_2 (Fig. 9). The deconvolution of the high resolution spectra of Ti $2p_{3/2}$ and O 1s confirms the presence of TiO_2 by the contributions found at 458.38 eV (Fig. 6b) and 529.72 eV (Fig. 6c), respectively. These peaks are characteristic of Ti $2p_{3/2}$ and O 1s in TiO_2 as already reported in previous studies [46,76,77,81–85]. A characteristic band for TiO_2 was also found in FTIR spectrum in the region between ~600–1200 cm^{-1} (Fig. 9). As shown in Fig. 6b the subpeak energy found for Ti $2p_{3/2}$ at 457.10 eV [76,86] is possibly related to Ti_2O_3 what is in accordance with the subpeak found for O 1s at 530.87 eV (Fig. 6d). Notwithstanding that, from curve fitting analysis of Ti $2p_{3/2}$ and O 1s main peaks, it is observed that the main contribution is coming from TiO_2. From Fig. 6d it is possible to identify a peak for F 1s at 683.98 eV, which is assigned to adsorbed fluoride ions on TiO_2 [46,87].

In Fig. 7a it is observed that C 1s was detected in NT-Ca/P samples at four different binding states namely at 284.42 eV (C—C groups), 285.85 eV (C—O groups), 287.74 (Organic C 1s), and finally, at 288.34 eV, which is possibly assigned to the presence of $CaCO_3$ [88]. Ti $2p_{3/2}$ components were found at 458.17 eV (TiO_2) and 457.16 eV (Ti_2O_3) as observed in Fig. 7b, and the O 1s binding energies for TiO_2 and Ti_2O_3 were detected at 529.55 eV and 530.30 eV, respectively (Fig. 7c). The O 1 s and Ca $2p_{3/2}$ core levels for $CaCO_3$ were found at 531.41 eV (Fig. 7c) and 346.3 eV (Fig. 7e), respectively [54]. Adsorbed fluoride ions on TiO_2 were detected at 683.78 eV (Fig. 7d). The anodization of TiO_2 nanotubes in Ca/P-electrolyte allowed the nanotubular surface enrichment with Ca and P elements. The Ca $2p_{3/2}$ peak detected at 346.89 eV (Fig. 7e), in agreement with P 1s peak at 132.9 eV (Fig. 7f), are most probably related to the presence of $Ca_3(PO_4)_2$ compounds on TiO_2 nanotubes [54,89]. Moreover, the energy found at 346. 30 eV may be also related with the presence of $CaHPO_4$ species, which were confirmed by the existence of a contribution for P 2p at 133.80 eV [54]. Furthermore, the O 1s binding energy at 531.3 eV (Fig. 7c) is corroborating the presence of $Ca_3(PO_4)_2/CaHPO_4$ species [54]. The presence of PO_4^{3-} groups can also be proved by the absorption peaks found in FTIR spectrum at 972.2 cm^{-1}, 1018.5 cm^{-1} and 1086.4 cm^{-1} (Fig. 9). Most likely, during anodization in Ca/P-electrolyte, Ca^{2+} ions reacted with neg-

atively charged PO_4^{3-} and CO_3^{2-} to form the Ca-based compounds above mentioned. Finally, it is believed that anodization of nanotubes leads to the formation of CaF_2 species as found by energies detected for Ca $2p_{3/2}$ and F 1s at 347.68 eV (Fig. 7e) and 684.35 eV (Fig. 7d), respectively [90]. C 1s species similar to those detected on NT-Ca/P were found also on NT-RP-Ca/P surfaces at similar binding energies (Fig. 8a). Once again, a high percentage of TiO_2 was detected in Ti $2p_{3/2}$ and O 1s spectra at 458.18 eV (Fig. 8b) and 529.55 eV (Fig. 8c), respectively. Ti_2O_3 was found in a lower at.% in Ti $2p_{3/2}$ spectrum at 457.13 eV (Fig. 8b) and at 530.7 eV in O1s spectrum (Fig. 8c). NT-RP-Ca/P surfaces were submitted to a reverse polarization step during 10 s in the Ca/P-electrolyte, in which, afterwards, they were immediately anodized at 100 V for 30 min. As observed in Figs. 7 and 8, similar compounds were detected on NT-RP-Ca/P comparing to NT-Ca/P surfaces, such as $CaCO_3$, $Ca_3(PO_4)_2$/$CaHPO_4$ and CaF_2. However, it should be noticed that an additional peak was found in Ca $2p_{3/2}$ spectrum at 346.20 eV (Fig. 8e) and it is most likely assigned to the presence of an additional chemical compound formed, namely, CaO. The O 1s core level for CaO was observed at 532.4 eV (Fig. 8c). These results indicate that reverse polarization is a promising treatment to be applied before anodization process leading possibly to the formation of additional compounds on materials surface, in this case, CaO on NT-RP-Ca/P surface.

The surface wettability is influenced by the surface characteristics such as surface roughness, chemistry and surface free energy [47,91–94]. Different elements are characterized by different surface energies, and so, the surface wettability depends on the surface energy of the elements. The higher the surface energy is, the higher the wetting [47,94]. In the present study, the hydrophilicity was enhanced after anodization of Ti as shown by the significant decrease in the WCA measured on Ti compared to NT surfaces (Table 3). This means that once a water droplet gets in contact with NT surfaces it completely expands on the entire surface. The hydrophilic character of these nanotubular structures is most probably related to the presence of OH groups adsorbed on its surface [95]. It is believed that the O 1s binding energy found for NT surfaces at around 531 eV (Fig. 6c) may be also assigned to OH groups adsorbed on TiO_2. Regonini et al. [77] after XPS analysis of TiO_2 nanotubular films synthesized by anodization, reported a certain degree of hydration in the oxide due to a signal typical of OH groups at 531.4 eV. TiO_2 nanotube arrays with OH groups adsorbed on its surface were also formed by Han et al. [66]. In agreement, absorption band from ~3000–3500 cm^{-1} found in FTIR spectrum (Fig. 9), is possibly attributed to fundamental stretching vibration of H_2O and OH groups. Earlier studies have focused on understanding the wettability behavior of titanium oxide nanotube surfaces. It has been reported that nanotubular films produced on Ti and Ti-alloys in EG-based electrolytes display superhydrophilic behavior [47,96]. Yoriya et al. [96] fabricated titania nanotubular films characterized by WCA of $13.8 \pm 2.2^\circ$ and stated that this was a clear indication of the superhydrophilic behavior of the nanotube layer. In the present work, the WCA measured for NT-Ca/P and NT-RP-Ca/P surfaces were $11.8 \pm 2.8^\circ$ and $10.5 \pm 3.0^\circ$, respectively (Table 3). These values are similar to the ones measured for NT surfaces and keep significantly lower than WCA of Ti. These results indicate that, beyond functionalization treatments of NT surfaces have influenced surface chemistry, their hydrophilic behavior remained unchanged. This feature may be of upmost importance once surface wettability plays a crucial role in cell adhesion, since this phase involves physicochemical linkages between cells and surfaces [16,31]. Besides, changes on surface wettability can lead to alterations in the adsorption of conditioning molecules influencing the cell attachment [31]. According to several studies, cells attach more efficiently to hydrophilic surfaces when compared to hydrophobic ones [16,31,97].

4.3. Corrosion behavior

The high corrosion resistance of Ti results from the growth of a protective TiO_2 film on its surface (2–6 nm thickness) [98]. However, this nano-thick passive layer is not inert to corrosive attack when subjected to aggressive biological conditions [24,25] (e.g. pH variation, presence of fluorides and surface wear). As a consequence of corrosion, metal ions may be released from a metallic implant to its vicinity impairing bone cell functions and triggering an immune response that can ultimately lead to periprosthetic resorption of bone and loosening of the implant [19,27,36]. Beyond metal ions accumulation in bone adjacent to implants, they have also been found to be localized in blood or serum, urine and other organs [99]. Thus, the study of how Ca/P-doped TiO_2 nanotubes behave when submitted to corrosive conditions is of upmost importance.

The electrochemical behavior of Ti, NT, NT-Ca/P and NT-RP-Ca/P samples was investigated in artificial saliva (AS) at 37 °C by potentiodynamic polarization. The electrochemical stability was assessed by the current values measured in the passive region (I_{pass}) of potentiodynamic polarization curves, whose values are shown in Table 4. The potentiodynamic polarization curves observed in Fig. 10 show that NT, NT-Ca/P and NT-RP-Ca/P samples exhibit a passive region extending over a wide potential range when compared to Ti surfaces. In general, all the nanotubular surfaces display a fast and effective passivation behavior, which may be related to the properties of the barrier layer formed at titanium/nanotubes interface during anodization process. The same trend was observed by Grotberg et al. [32] for nanotubes grown from Ti6Al4 V substrates. Yu et al. [33] also studied the corrosion behavior of TiO_2 nanotube layers in Hank's solution and they concluded that the I_{pass} density was significantly influenced by Ti oxide nanotubes grown by anodization. Electrochemical Impedance Spectroscopy (EIS) results confirmed the better corrosion resistance of Ti nanotubes because of a thicker barrier layer present on nanotubular films than on smooth Ti. The passive layer grown during anodization process plays the main role in corrosion restricting the movement of metal ions from the metallic surface to the surrounding solution [100]. Likewise, Demestrescu et al. [101] studied the effect of nano-topographical features of Ti/TiO_2 electrode surface on its electrochemical stability in Fusayama's AS. From EIS and potentiodynamic studies, the authors concluded that very low corrosion current densities were recorded on TiO_2 nanotubes due to a strong passive oxide film formation. The EIS results indicated that TiO_2 nanotube surface consisted of a bi-layered oxide made up of an inner barrier layer associated to high impedance and responsible for corrosion protection, and a porous outer layer (nanotubes) of lower impedance.

Beyond the faster passivation behavior of NT samples, similar I_{pass} values were found for smooth Ti, as observed in Fig. 10 and confirmed by the I_{pass} values reported in Table 4. However, after Ca- and P-enrichment of NT surfaces by anodization and reverse polarization processes, significantly lower I_{pass} values were found for NT-Ca/P and NT-RP-Ca/P samples (Fig. 10, Table 4) suggesting that they display superior corrosion resistance ability. From NT-Ca/P and NT-RP-Ca/P polarization curves, it is believed that this abrupt decrease in the I_{pass} values is related to the barrier layer at titanium/nanotubes interface, whose properties might have been changed during the anodization of NT surfaces in the Ca/P-electrolyte. During the second anodization process it is hypothesized that the diffusion of anionic oxygen species occurs through the nanotubes and the already existing passive layer, and reacts with Ti ions liberated from the titanium substrate to form a compact oxide film providing superior corrosion resistance.

Recently, Yu et al. [102] reported on a method to enhance the adhesion of TiO_2 arrays to Ti substrate by employing an additional anodization of nanotubes in a fluoride-free organic electrolyte constituted of H_3PO_4 and EG. The additional anodization resulted in about 200 nm thick compact layer near the nanotube bottoms and scratch test demonstrated that this layer leads to a more than three-fold increase of the adhesion strength between the nanotubes and the substrate. It is important to highlight that the morphological features of all the nanotubular surfaces remained unaltered after corrosion assays, as confirmed by FESEM observation of the surface area exposed to AS (results not shown).

From the results obtained it appears that the lowering on the I_{pass} values is not affected by the reverse polarization step, which led to the significant reduction of the nanotube length as discussed in Section 4.1, and so, it is also independent of nanotube length. Furthermore, all the nanotubular surfaces are superhydrophilic and characterized by similar values of WCA, and so, it seems that I_{pass} values are also independent on this feature. This indicates that the barrier layer formed at titanium/nanotube interface is the main cause for the significant I_{pass} lowering. The characterization of the newly formed titanium/nanotubes interface after anodization of nanotubes in Ca/P-electrolyte regarding compact layer morphology, thickness and elemental composition is of upmost importance. This knowledge will allow to predict the mechanisms behind the barrier layer formation and to understand the properties responsible for the improved corrosion resistance of Ca/P-doped TiO_2 nanotubes.

4.4. Adhesion and proliferation of MG-63 cells

Ideally, the biological fixation between an implant surface and the surrounding bone should occur ensuring the establishment of a mechanically solid interface without fibrous tissue formation [35,37,103], however, this is still one of the main challenges that researchers aim to overcome [34]. This present study uses a novel surface functionalization strategy to provide a biomimetic surface. The new adopted methodology aims to tailor more effective bone-integrating surfaces by mimicking the morphology of natural bone at a nano-scale level, as well as its composition through the enrichment of the TiO_2 nanotubes with Ca and P species.

From the results described in Section 3.3, all the nanotubular surfaces influenced the cell responses regarding cell adhesion and proliferation. In accordance with FESEM observation of MG-63 cells after one day of incubation (Fig. 11 a1, b1, c1 and d1), the cells adhered on TiO_2 nanotube surfaces presented a spreader morphology with filopodia forming adhesion points and promoting cell–cell contact through cytoplasmic extensions, compared to smooth Ti. Moreover, the metabolic activity of cells measured by MTT assay after six days of culture (Fig. 13), suggests that NT surfaces induced to a significantly higher proliferation of MG-63 cells than smooth Ti [104,105]. These outcomes may be related to the more rapid adhesion and spreading of osteoblastic cells on NT surfaces as also observed by Oh et al. [105]. Cell adhesion is one of the critical initial stages to subsequent proliferation of osteoblastic cells producers of bony tissue, playing a crucial role in the establishment of a high bone-implant contact [11,106,107].

Cell-substrate adhesion is based on membrane integrins (8–12 nm), which are essential for the formation of focal adhesion points with the implant surface [108]. Integrins can translate the attachment of external ligands (e.g. fibronectin and vitronectin) to internal information that induces adhesion, spreading, cell migration, growth and differentiation [109]. It has been already shown that TiO_2 nanotubes influence cell proliferation, migration and differentiation resulting from integrin clustering and focal contact formation [108], and these responses depend on nanotube features such as diameter and wall thickness. However, the cell response to different TiO_2 nanotube diameters is still controversial in literature. Nanotubes with 15–30 nm promote cell adhesion and proliferation and, on the other hand, nanotubes with 70–100 nm are believed to induce a greater bone forming ability [109]. Brammer et al. [104] prepared various sizes (30–100 nm diameter) of TiO_2 nanotubes on Ti substrates by anodization, and investigated the osteoblast cellular behavior in response to these different nanotube sizes. The experimental data indicated that a substantially increased elongation of the cells when cultured on 100 nm diameter nanotubes was achieved with cell differentiation ability, when compared to flat Ti. In the present work, TiO_2 nanotubes with diameter ranging from 45 to 90 nm and a wall thickness from 14 to 24 nm were produced. The improved cell adhesion and proliferation of MG-63 cells adhered on NT surfaces is probably related with these nanofeatures of the tubes that influence cell adhesion process through integrin receptors, as mentioned previously. Furthermore, it has been reported that cells adhere better on hydrophilic surfaces and with functional groups such as OH^- [110], which are characteristics of NT surfaces when compared to Ti. Additionally, F ions adsorbed on NT surfaces, may be stimulating initial cell attachment [108]. Thus, it is believed that the surface features of NT surfaces as morphology and chemistry are beneficial for the initial protein adsorption and subsequent cell adhesion process when compared to smooth Ti.

Different behaviors regarding cell adhesion quality and proliferation were observed for osteoblastic cells seeded on NT-Ca/P and NT-RP-Ca/P surfaces. After six days of culture, osteoblastic cells seeded on NT-RP-Ca/P surfaces presented a spreader and more stretched morphology compared to the ones on NT-Ca/P surfaces (Fig. 12 d2 *vs* c2) as well as an enhanced metabolic activity (Fig. 13). In Fig. 12 d1 and d2 it is observed that there is an increased number of adhered cells on NT-RP-Ca/P surfaces through the culture time. However, the same behavior is not observed on NT-Ca/P surfaces (Fig. 12 c1 and c2,), where there is not an increase on the amount of MG-63 cells, which in turns are more scarcely distributed presenting a rounder morphology. The MTT results are in good agreement with these observations, showing a significantly lower metabolic activity of the adhered cells on NT-Ca/P compared to NT-RP-Ca/P surfaces, suggesting a lower proliferation. Cell to cell contacts are quite observed on NT-RP-Ca/P surfaces through filopodia, which are also observed traveling along the nanotubes. The differences on cellular responses found between NT-Ca/P and NT-RP-Ca/P surfaces are most probably related to their chemical features, which were changed after reverse polarization step. As known from literature, surface chemistry plays an important role in cell adhesion because it influences short-term adhesion, which is a step that involves adsorption and rearrangement of proteins [110]. From chemical analysis of NT-RP-Ca/P surfaces it was found the presence of $Ca_3(PO_4)_2$/$CaHPO_4$, CaF_2, $CaCO_3$ and CaO species. These compounds were also found on NT-Ca/P surfaces with the exception of CaO. According to the findings by Dorner-Reisel et al. [111], an alteration of the biological acceptance of Diamond-Like Carbon (DLC) films was induced by CaO incorporation. In accordance with the authors, the DLC doping with CaO led to an improvement on cell morphology and viability. In the present study, the formation of CaO may be acting as a determining factor, influencing the initial adherence of proteins on the surface, and consequently, the cell adhesion and proliferation. However, further studies must be carried out to confirm this hypothesis.

From the results above discussed, it appears that the anodization of nanotubes in Ca/P-electrolyte is modulating cell responses and that reverse polarization is a very promising strategy for the design of new osseointegrative surfaces. The reverse polarization step before anodization in the Ca/P-electrolyte helps to recover the biological functions of cells adhered on NT surfaces regarding metabolic cell activity and cell adhesion. This suggests that beyond morphological/topographical features, cells seem to respond to

chemical properties of TiO_2 nanotubes. Further studies still need to be carried out aiming to understand better the mechanisms governing cell adhesion and proliferation on these surfaces. Furthermore, cell differentiation studies would be also of fundamental importance to perform, aiming to understand if Ca/P-doped TiO_2 nanotubes have potential to modulate osteogenesis.

5. Conclusions

The synthesis of biocompatible Ca/P-doped TiO_2 nanotubes was successfully achieved with improved electrochemical behavior in AS. The main conclusions of this investigation are as follows:

- Highly ordered TiO_2 nanotubes were synthesized by two-step anodizing treatments. The nanotubes are characterized by non-uniform diameters varying at a nano-scale level from 50 to 90 nm, presenting a very similar morphology when compared to the micron structure of natural bone.
- Reverse polarization of highly ordered TiO_2 nanotubes in a Ca/P-electrolyte, followed by anodization in the same electrolyte, leads to a nanotubular film enriched with bioactive elements namely, Ca and P. The functionalization treatment by reverse polarization before anodization does not affect the morphology of the nanotubes, however, it influences their chemical properties.
- Reverse polarization in Ca/P-electrolyte improves the biocompatibility of Ca/P-doped TiO_2. By this novel approach, the chemistry of TiO_2 nanotubes may be modified without compromising the desired surface morphological features.
- Ca/P-doped TiO_2 nanotubes display a significantly lower passive current than NT and smooth Ti samples in AS at 37 °C. The anodization of TiO_2 nanotubes in Ca/P-electrolyte seems to be a promising and simple approach to improve the electrochemical stability of metallic implants and avoid their degradation by corrosion.

The present study brings up a novel methodology that relies on the bio-functionalization of TiO_2 nanotubes by the conjugation of reverse polarization and anodization processes in a Ca/P-electrolyte. This new strategy allows the synthesis of bone-like structured TiO_2 nanotubes enriched with bioactive elements, able to enhance osteoblastic cell functions and simultaneously, to minimize their degradation by corrosion. This study addresses a very promising and simple approach providing new insights for the further development of novel methodologies to improve the outcome of dental and orthopedic implants.

Acknowledgements

This work made use of the facilities at the Electron Microscopy Service (Research Resource Center, UIC). The authors would like to thank the financial support provided by the Department of Bioengineering of the University of Illinois at Chicago; the National Science Foundation for the DMR Grant # 1564950 and NSF Grant #1067424; the Portuguese Foundation for Science and Technology for the doctoral grant (Ref. SFRH/BD/88517/2012); the National Council for Scientific and Technological Development for the grant (Ref. 490761/2013-5); and the Coordination for the Improvement of Higher Education Personnel for the financial support (Ref. 99999.008666/2014-08).

References

[1] Y. Oshida, E.B. Tuna, O. Aktören, K. Gençay, Dental implant systems, Int. J. Mol. Sci. 11 (2010) 1580–1678.
[2] P.A. Norowski, J.D. Bumgardner, Biomaterial and antibiotic strategies for peri-implantitis, J. Biomed. Mater. Res. Part B-Appl. Biomater. 88B (2009) 530–543.
[3] T.D. Taylor, Prosthodontic problems and limitations associated with osseointegration, J. Prosthet. Dent. 79 (1998) 74–78.
[4] J. Park, S. Bauer, K.A. Schlegel, F.W. Neukam, K. von der Mark, P. Schmuki, TiO2 nanotube surfaces: 15 nm—an optimal length scale of surface topography for cell adhesion and differentiation, Small 5 (2009) 666–671.
[5] A.C. Vieira, A.R. Ribeiro, L.A. Rocha, J.P. Celis, Influence of pH and corrosion inhibitors on the tribocorrosion of titanium in artificial saliva, Wear 261 (2006) 994–1001.
[6] N. Wang, H. Li, W. Lü, J. Li, J. Wang, Z. Zhang, Y. Liu, Effects of TiO 2 nanotubes with different diameters on gene expression and osseointegration of implants in minipigs, Biomaterials 32 (2011) 6900–6911.
[7] R. Kane, P.X. Ma, Mimicking the nanostructure of bone matrix to regenerate bone, Mater. Today 16 (2013) 418–423.
[8] N. Ibrahim, A. Parsa, B. Hassan, P. van der Stelt, D. Wismeijer, Diagnostic imaging of trabecular bone microstructure for oral implants: a literature review, Dentomaxillofacial Radiol. 42 (2013) 20120075.
[9] K. Indira, U.K. Mudali, N. Rajendran, Corrosion behavior of electrochemically assembled nanoporous titania for biomedical applications, Ceram. Int. 39 (2013) 959–967.
[10] L. Zhao, H. Wang, K. Huo, X. Zhang, W. Wang, Y. Zhang, Z. Wu, P.K. Chu, The osteogenic activity of strontium loaded titania nanotube arrays on titanium substrates, Biomaterials 34 (2013) 19–29.
[11] L. Le Guehennec, M.A. Lopez-Heredia, B. Enkel, P. Weiss, Y. Amouriq, P. Layrolle, Osteoblastic cell behaviour on different titanium implant surfaces, Acta Biomater. 4 (2008) 535–543.
[12] R.A. Surmenev, M.A. Surmeneva, A.A. Ivanova, Significance of calcium phosphate coatings for the enhancement of new bone osteogenesis—a review, Acta Biomater. 10 (2014) 557–579.
[13] A. Ribeiro, F. Oliveira, L. Boldrini, P. Leite, P. Falagan-Lotsch, A. Linhares, W. Zambuzzi, B. Fragneaud, A. Campos, C. Gouvêa, Micro-arc oxidation as a tool to develop multifunctional calcium-rich surfaces for dental implant applications, Mater. Sci. Eng.: C 54 (2015) 196–206.
[14] H. Cao, H. Qin, Y. Zhao, G. Jin, T. Lu, F. Meng, X. Zhang, X. Liu, Nano-thick calcium oxide armed titanium: boosts bone cells against methicillin-resistant Staphylococcus aureus, Sci. Rep. (2016) 6.
[15] I. Demetrescu, C. Pirvu, V. Mitran, Effect of nano-topographical features of Ti/TiO2 electrode surface on cell response and electrochemical stability in artificial saliva, Bioelectrochemistry 79 (2010) 122–129.
[16] K. Das, S. Bose, A. Bandyopadhyay, Surface modifications and cell-materials interactions with anodized Ti, Acta Biomater. 3 (2007) 573–585.
[17] B. Klinge, M. Hultin, T. Berglundh, Peri-implantitis, Dent. Clin. North Am. 49 (2005) 661–676 (vii-viii).
[18] P.A. Norowski, J.D. Bumgardner, Biomaterial and antibiotic strategies for peri-implantitis: a review, J. Biomed. Mater. Res. B Appl. Biomater. 88B (2009) 530–543.
[19] H.-J. Song, M.-K. Kim, G.-C. Jung, M.-S. Vang, Y.-J. Park, The effects of spark anodizing treatment of pure titanium metals and titanium alloys on corrosion characteristics, Surf. Coat. Technol. 201 (2007) 8738–8745.
[20] K. Gulati, S. Ramakrishnan, M.S. Aw, G.J. Atkins, D.M. Findlay, D. Losic, Biocompatible polymer coating of titania nanotube arrays for improved drug elution and osteoblast adhesion, Acta Biomater. 8 (2012) 449–456.
[21] G.A. Crawford, N. Chawla, J.E. Houston, Nanomechanics of biocompatible TiO2 nanotubes by interfacial force microscopy (IFM), J. Mech. Behav. Biomed. Mater. 2 (2009) 580–587.
[22] S. Minagar, C.C. Berndt, J. Wang, E. Ivanova, C. Wen, A review of the application of anodization for the fabrication of nanotubes on metal implant surfaces, Acta Biomater. 8 (2012) 2875–2888.
[23] T. Albrektsson, C. Johansson, Osteoinduction, osteoconduction and osseointegration, Eur. Spine J. 10 (Suppl. 2) (2001) S96–101.
[24] M.T. Mathew, S. Abbey, N.J. Hallab, D.J. Hall, C. Sukotjo, M.A. Wimmer, Influence of pH on the tribocorrosion behavior of CpTi in the oral environment: synergistic interactions of wear and corrosion, J. Biomed. Mater. Res. B 100B (2012) 1662–1671.
[25] M.T. Mathew, V.A. Barão, J.C.-C. Yuan, W.G. Assunção, C. Sukotjo, M.A. Wimmer, What is the role of lipopolysaccharide on the tribocorrosive behavior of titanium, J. Mech. Behav. Biomed. Mater. 8 (2012) 71–85.
[26] X. Liu, P.K. Chu, C. Ding, Surface nano-functionalization of biomaterials, Mater. Sci. Eng. R.: Rep. 70 (2010) 275–302.
[27] S. Faghihi, D. Li, J.A. Szpunar, Tribocorrosion behaviour of nanostructured titanium substrates processed by high-pressure torsion, Nanotechnology 21 (2010) 485703.
[28] L. Le Guehennec, A. Soueidan, P. Layrolle, Y. Amouriq, Surface treatments of titanium dental implants for rapid osseointegration, Dent. Mater. 23 (2007) 844–854.
[29] M. Jayaraman, U. Meyer, M. Bühner, U. Joos, H.-P. Wiesmann, Influence of titanium surfaces on attachment of osteoblast-like cells in vitro, Biomaterials 25 (2004) 625–631.
[30] G.B. de Souza, G.G. de Lima, N.K. Kuromoto, P. Soares, C.M. Lepienski, C.E. Foerster, A. Mikowski, Tribo-mechanical characterization of rough, porous and bioactive Ti anodic layers, J. Mech. Behav. Biomed. Mater. 4 (2011) 796–806.
[31] X. Zhu, J. Chen, L. Scheideler, R. Reichl, J. Geis-Gerstorfer, Effects of topography and composition of titanium surface oxides on osteoblast responses, Biomaterials 25 (2004) 4087–4103.
[32] J. Grotberg, A. Hamlekhan, A. Butt, S. Patel, D. Royhman, T. Shokuhfar, C. Sukotjo, C. Takoudis, M.T. Mathew, Thermally oxidized titania nanotubes

enhance the corrosion resistance of Ti6Al4V, Mater. Sci. Eng.: C 59 (2016) 677–689.
[33] W.-Q. Yu, J. Qiu, L. Xu, F.-Q. Zhang, Corrosion behaviors of TiO2 nanotube layers on titanium in Hank's solution, Biomed. Mater. 4 (2009) 065012.
[34] T.K. Monsees, K. Barth, S. Tippelt, K. Heidel, A. Gorbunov, W. Pompe, R.H. Funk, Effects of different titanium alloys and nanosize surface patterning on adhesion, differentiation, and orientation of osteoblast-like cells, Cells Tissues Organs 180 (2005) 81–95.
[35] K. Anselme, Osteoblast adhesion on biomaterials, Biomaterials 21 (2000) 667–681.
[36] N. Cobelli, B. Scharf, G.M. Crisi, J. Hardin, L. Santambrogio, Mediators of the inflammatory response to joint replacement devices, Nat. Rev. Rheumatol. 7 (2011) 600–608.
[37] A.B. Novaes Jr., S.L. de Souza, R.R. de Barros, K.K. Pereira, G. Iezzi, A. Piattelli, Influence of implant surfaces on osseointegration, Braz. Dent. J. 21 (2010) 471–481.
[38] Z. Cheng, F. Zhang, F. He, L. Zhang, C. Guo, S. Zhao, G. Yang, Osseointegration of titanium implants with a roughened surface containing hydride ion in a rabbit model, Oral Surg. Oral Med. Oral Pathol. Oral Radiol. Endod. 110 (2010) e5–12.
[39] G. Mendonca, D.B. Mendonca, L.G. Simoes, A.L. Araujo, E.R. Leite, W.R. Duarte, F.J. Aragao, L.F. Cooper, The effects of implant surface nanoscale features on osteoblast-specific gene expression, Biomaterials 30 (2009) 4053–4062.
[40] K.S. Brammer, C.J. Frandsen, S. Jin, TiO2 nanotubes for bone regeneration, Trends Biotechnol. 30 (2012) 315–322.
[41] S. Minagar, Y. Li, C.C. Berndt, C. Wen, The influence of titania-zirconia-zirconium titanate nanotube characteristics on osteoblast cell adhesion, Acta Biomater. 12 (2015) 281–289.
[42] S. Alves, R. Bayón, V.S. de Viteri, M. Garcia, A. Igartua, M. Fernandes, L. Rocha, Tribocorrosion behavior of calcium-and phosphorous-enriched titanium oxide films and study of osteoblast interactions for dental implants, J. Bio-Tribo-Corros. 1 (2015) 1–21.
[43] T. Fusayama, T. Katayori, S. Nomoto, Corrosion of Gold and Amalgam Placed in Contact WithEach Other, 1963.
[44] S. Komasa, Y. Taguchi, H. Nishida, M. Tanaka, T. Kawazoe, Bioactivity of nanostructure on titanium surface modified by chemical processing at room temperature, J. Prosthodont. Res. 56 (2012) 170–177.
[45] A. Dementjev, A. DeGraaf, M. VandeSanden, K. Maslakov, A. Naumkin, A. Serov, X-ray photoelectron spectroscopy reference data for identification of the C 3N 4 phase in carbon-nitrogen films, Diamond Relat. Mater. 9 (2000) 1904–1907.
[46] R.P. Antony, T. Mathews, S. Dash, A.K. Tyagi, B. Raj, X-ray photoelectron spectroscopic studies of anodically synthesized self aligned TiO2 nanotube arrays and the effect of electrochemical parameters on tube morphology, Mater. Chem. Phys. 132 (2012) 957–966.
[47] S.B. Patel, A. Hamlekhan, D. Royhman, A. Butt, J. Yuan, T. Shokuhfar, C. Sukotjo, M.T. Mathew, G. Jursich, C.G. Takoudis, Enhancing surface characteristics of Ti-6Al-4 V for bio-implants using integrated anodization and thermal oxidation, J. Mater. Chem. B 2 (2014) 3597–3608.
[48] D. Yates, Infrared studies of the surface hydroxyl groups on titanium dioxide, and of the chemisorption of carbon monoxide and carbon dioxide, J. Phys. Chem. 65 (1961) 746–753.
[49] A. Hamlekhan, A. Butt, S. Patel, D. Royhman, C. Takoudis, C. Sukotjo, J. Yuan, G. Jursich, M.T. Mathew, W. Hendrickson, Fabrication of anti-aging TiO2 nanotubes on biomedical Ti alloys, PLoS One 9 (2014) e96213.
[50] T. Bezrodna, G. Puchkovska, V. Shymanovska, J. Baran, H. Ratajczak, IR-analysis of H-bonded H2O on the pure TiO2 surface, J. Mol. Struct. 700 (2004) 175–181.
[51] D.C.L. Vasconcelos, E.H.M. Nunes, M. Gasparon, W.L. Vasconcelos, Infrared spectroscopy of titania sol-gel coatings on 316L stainless steel, Mater. Sci. Appl. 2 (2011) 1375.
[52] I. Becker, I. Hofmann, F.A. Müller, Preparation of bioactive sodium titanate ceramics, J. Eur. Ceram. Soc. 27 (2007) 4547–4553.
[53] X.-B. Chen, Y.-C. Li, J.D. Plessis, P.D. Hodgson, C.E. Wen, Influence of calcium ion deposition on apatite-inducing ability of porous titanium for biomedical applications, Acta Biomater. 5 (2009) 1808–1820.
[54] A. Roguska, M. Pisarek, M. Andrzejczuk, M. Dolata, M. Lewandowska, M. Janik-Czachor, Characterization of a calcium phosphate-TiO2 nanotube composite layer for biomedical applications, Mater. Sci. Eng.: C 31 (2011) 906–914.
[55] M. Goudarzi, F. Batmanghelich, A. Afshar, A. Dolati, G. Mortazavi, Development of electrophoretically deposited hydroxyapatite coatings on anodized nanotubular TiO2 structures: corrosion and sintering temperature, Appl. Surf. Sci. 301 (2014) 250–257.
[56] M. Pisarek, A. Roguska, L. Marcon, M. Andrzejczuk, Biomimetic and electrodeposited calcium-phosphates coatings on Ti - formation, surface characterization, biological response, in: R. Hudak, M. Penhaker, J. Majernik (Eds.), Biomedical Engineering - Technical Applications in Medicine, InTech, 2012, ISBN.
[57] Y. Yajing, D. Qiongqiong, H. Yong, S. Han, X. Pang, Magnesium substituted hydroxyapatite coating on titanium with nanotublar TiO2 intermediate layer via electrochemical deposition, Appl. Surf. Sci. 305 (2014) 77–85.
[58] L. Berzina-Cimdina, N. Borodajenko, Research of calcium phosphates using Fourier transform infrared spectroscopy, in: Theophile Theophanides (Ed.), Infrared Spectroscopy Materials Science, Engineering and Technology, 2012, pp. 123–149.
[59] A. Roguska, S. Hiromoto, A. Yamamoto, M.J. Woźniak, M. Pisarek, M. Lewandowska, Collagen immobilization on 316L stainless steel surface with cathodic deposition of calcium phosphate, Appl. Surf. Sci. 257 (2011) 5037–5045.
[60] S. Wang, Y. Liu, C. Zhang, Z. Liao, W. Liu, The improvement of wettability, biotribological behavior and corrosion resistance of titanium alloy pretreated by thermal oxidation, Tribol. Int. 79 (2014) 174–182.
[61] V.S. Saji, H.C. Choe, W.A. Brantley, An electrochemical study on self-ordered nanoporous and nanotubular oxide on Ti-35Nb-5Ta-7Zr alloy for biomedical applications, Acta Biomater. 5 (2009) 2303–2310.
[62] S. Takahashi, T. Abe, J. Gotoh, Y. Fukuuchi, Substrate-dependence of reduction of MTT: a tetrazolium dye differs in cultured astroglia and neurons, Neurochem. Int. 40 (2002) 441–448.
[63] J. Fojt, H. Moravec, L. Joska, Nanostructuring of titanium for medical applications. nanocon 2010, 2nd International Conference (2010) 209–213.
[64] S. Grigorescu, V. Pruna, I. Titorencu, V.V. Jinga, A. Mazare, P. Schmuki, I. Demetrescu, The two step nanotube formation on TiZr as scaffolds for cell growth, Bioelectrochemistry 98 (2014) 39–45.
[65] D. Regonini, C.R. Bowen, A. Jaroenworaluck, R. Stevens, A review of growth mechanism, structure and crystallinity of anodized TiO2 nanotubes, Mater. Sci. Eng. R.: Rep. 74 (2013) 377–406.
[66] S. Han, J. Doh, J. Yoon, G. Kim, J. Byun, S. Han, K. Hong, S. Kwun, Highly ordered self-organized TiO2 nanotube arrays prepared by a multi-step anodic oxidation process, Met. Mater. Int. 15 (2009) 493–499.
[67] T. Serikov, N.K. Ibrayev, V. Gladkova, Synthesis and investigation of the geometric characteristics of titanium dioxide nanotubes, in: IOP Conference Series: Materials Science and Engineering, IOP Publishing, 2015, pp. 012121.
[68] G.D. Sulka, J. Kapusta-Kołodziej, A. Brzózka, M. Jaskuła, Anodic growth of TiO2 nanopore arrays at various temperatures, Electrochim. Acta 104 (2013) 526–535.
[69] S. Grigorescu, C. Ungureanu, R. Kirchgeorg, P. Schmuki, I. Demetrescu, Various sized nanotubes on TiZr for antibacterial surfaces, Appl. Surf. Sci. 270 (2013) 190–196.
[70] G. Sulka, S. Stroobants, V. Moshchalkov, G. Borghs, J.-P. Celis, Effect of tensile stress on growth of self-organized nanostructures on anodized aluminum, J. Electrochem. Soc. 151 (2004) B260–B264.
[71] Y. Hu, K.Y. Cai, Z. Luo, D.W. Xu, D.C. Xie, Y.R. Huang, W.H. Yang, P. Liu, TiO2 nanotubes as drug nanoreservoirs for the regulation of mobility and differentiation of mesenchymal stem cells, Acta Biomater. 8 (2012) 439–448.
[72] E. Peláez Abellán, L. Rocha-Souza, A. Guastaldi, Cathodic behaviour of anodized titanium in simulated physiological, Latin Am. Appl. Res. 41 (2011) 199–203.
[73] R. Torresi, O. Camara, C. De Pauli, Influence of the hydrogen evolution reaction on the anodic titanium oxide film properties, Electrochim. Acta 32 (1987) 1357–1363.
[74] M. Vezvaie, J. Noël, Z. Tun, D. Shoesmith, Hydrogen absorption into titanium under cathodic polarization: an in-situ neutron reflectometry and EIS study, J. Electrochem. Soc. 160 (2013) C414–C422.
[75] D. Kowalski, D. Kim, P. Schmuki, TiO2 nanotubes, nanochannels and mesosponge: self-organized formation and applications, Nano Today 8 (2013) 235–264.
[76] A. Roguska, M. Pisarek, M. Andrzejczuk, M. Dolata, M. Lewandowska, M. Janik-Czachor, Characterization of a calcium phosphate-TiO 2 nanotube composite layer for biomedical applications, Mater. Sci. Eng.: C 31 (2011) 906–914.
[77] D. Regonini, A. Jaroenworaluck, R. Stevens, C.R. Bowen, Effect of heat treatment on the properties and structure of TiO2 nanotubes: phase composition and chemical composition, Surf. Interface Anal. 42 (2010) 139–144.
[78] H. Shin, J. Jung, S. Kim, W. Lee, XPS analysis on chemical properties of calcium phosphate thin films and osteoblastic HOS cell responses, J. Ind. Eng. Chem.-Seoul 12 (2006) 476.
[79] H. Jensen, A. Soloviev, Z. Li, E.G. Søgaard, XPS and FTIR investigation of the surface properties of different prepared titania nano-powders, Appl. Surf. Sci. 246 (2005) 239–249.
[80] P.A. Mangrulkar, S.P. Kamble, M.M. Joshi, J.S. Meshram, N.K. Labhsetwar, S.S. Rayalu, Photocatalytic degradation of phenolics by N-doped mesoporous titania under solar radiation, Int. J. Photoenergy (2011) 2012.
[81] K. Raja, T. Gandhi, M. Misra, Effect of water content of ethylene glycol as electrolyte for synthesis of ordered titania nanotubes, Electrochem. Commun. 9 (2007) 1069–1076.
[82] C.A. Grimes, G.K. Mor, Material properties of TiO2 nanotube arrays: structural, elemental, mechanical, optical and electrical, in: TiO2 Nanotube Arrays, Springer, 2009, pp. 67–113.
[83] K. Indira, U.K. Mudali, N. Rajendran, In-vitro biocompatibility and corrosion resistance of strontium incorporated TiO2 nanotube arrays for orthopaedic applications, J. Biomater. Appl. 29 (2014) 113–129.
[84] R. Hang, Y. Liu, S. Liu, L. Bai, A. Gao, X. Zhang, X. Huang, B. Tang, P.K. Chu, Size-dependent corrosion behavior and cytocompatibility of Ni-Ti-O nanotubes prepared by anodization of biomedical NiTi alloy, Corros. Sci. 103 (2015) 173–180.
[85] S. Sreekantan, K.A. Saharudin, Z. Lockman, T.W. Tzu, Fast-rate formation of TiO2 nanotube arrays in an organic bath and their applications in photocatalysis, Nanotechnology 21 (2010) 365603.

[86] M. Pisarek, A. Roguska, L. Marcon, M. Andrzejczuk, Biomimetic and electrodeposited calcium-Phosphates coatings on Ti-Formation, in: Surface Characterization, Biological Response, INTECH Open Access Publisher, 2012.
[87] K.G. Neoh, X. Hu, D. Zheng, E.T. Kang, Balancing osteoblast functions and bacterial adhesion on functionalized titanium surfaces, Biomaterials 33 (2012) 2813–2822.
[88] R. Raliya, A. Som, N. Shetty, N. Reed, S. Achilefu, P. Biswas, Nano-antacids enhance pH neutralization beyond their bulk counterparts: synthesis and characterization, RSC Adv. 6 (2016) 54331–54335.
[89] M. Bigerelle, K. Anselme, B. Noël, I. Ruderman, P. Hardouin, A. Iost, Improvement in the morphology of Ti-based surfaces: a new process to increase in vitro human osteoblast response, Biomaterials 23 (2002) 1563–1577.
[90] W. Fu, S. Ding, Y. Wang, L. Wu, D. Zhang, Z. Pan, R. Wang, Z. Zhang, S. Qiu, F Ca co-doped TiO 2 nanocrystals with enhanced photocatalytic activity, Dalton Trans. 43 (2014) 16160–16163.
[91] F. Rupp, L. Scheideler, D. Rehbein, D. Axmann, J. Geis-Gerstorfer, Roughness induced dynamic changes of wettability of acid etched titanium implant modifications, Biomaterials 25 (2004) 1429–1438.
[92] Y.J. Lim, Y. Oshida, C.J. Andres, M.T. Barco, Surface characterizations of variously treated titanium materials, Int. J. Oral Maxillofac. Implants 16 (2000) 333–342.
[93] B. Bhushan, Y. Chae Jung, Wetting study of patterned surfaces for superhydrophobicity, Ultramicroscopy 107 (2007) 1033–1041.
[94] F. Rupp, R.A. Gittens, L. Scheideler, A. Marmur, B.D. Boyan, Z. Schwartz, J. Geis-Gerstorfer, A review on the wettability of dental implant surfaces I: Theoretical and experimental aspects, Acta Biomater. 10 (2014) 2894–2906.
[95] D.H. Shin, T. Shokuhfar, C.K. Choi, S.-H. Lee, C. Friedrich, Wettability changes of TiO2 nanotube surfaces, Nanotechnology 22 (2011) 315704.
[96] S. Yoriya, W. Kittimeteeworakul, N. Punprasert, Effect of anodization parameters on morphologies of TiO2 nanotube arrays and their surface properties, J. Chem. Eng. 6 (2012) 686–691.
[97] Z. Artzi, C.E. Nemcovsky, H. Tal, E. Weinberg, M. Weinreb, H. Prasad, M.D. Rohrer, A. Kozlovsky, Clinical and histomorphometric observations around dual acid-etched and calcium phosphate nanometer deposited-surface implants, Int. J. Oral Maxillofac. Implants 26 (2011) 893–901.
[98] L. Yang, V. Chinthapenta, Q. Li, D. Stout, A. Liang, B.W. Sheldon, T.J. Webster, Understanding osteoblast responses to stiff nanotopographies through experiments and computational simulations, J. Biomed. Mater. Res. A 97 (2011) 375–382.
[99] Z.L. Sun, J.C. Wataha, C.T. Hanks, Effects of metal ions on osteoblastlike cell metabolism and differentiation, Gene Expr. 11 (1997) 12.
[100] X. Yu, Y. Li, W. Wlodarski, S. Kandasamy, K. Kalantar-zadeh, Fabrication of nanostructured TiO2 by anodization: a comparison between electrolytes and substrates, Sens. Actuators B 130 (2008) 25–31.
[101] I. Demetrescu, C. Pirvu, V. Mitran, Effect of nano-topographical features of Ti/TiO 2 electrode surface on cell response and electrochemical stability in artificial saliva, Bioelectrochemistry 79 (2010) 122–129.
[102] D. Yu, X. Zhu, Z. Xu, X. Zhong, Q. Gui, Y. Song, S. Zhang, X. Chen, D. Li, Facile method to enhance the adhesion of TiO2 nanotube arrays to Ti substrate, ACS Appl. Mater. Interfaces 6 (2014) 8001–8005.
[103] S. Kaneco, Y. Chen, P. Westerhoff, J.C. Crittenden, Fabrication of uniform size titanium oxide nanotubes: impact of current density and solution conditions, Scr. Mater. 56 (2007) 373–376.
[104] F. Ravanetti, P. Borghetti, E. De Angelis, R. Chiesa, F.M. Martini, C. Gabbi, A. Cacchioli, In vitro cellular response and in vivo primary osteointegration of electrochemically modified titanium, Acta Biomater. 6 (2010) 1014–1024.
[105] A.P. Tomisa, M.E. Launey, J.S. Lee, M.H. Mankani, U.G. Wegst, E. Saiz, Nanotechnology approaches to improve dental implants, Int. J. Oral Maxillofac. Implants 26 (Suppl) (2011) 25–44 (discussion 5–9).
[106] S. Oh, C. Daraio, L.-H. Chen, T.R. Pisanic, R.R. Fiñones, S. Jin, Significantly accelerated osteoblast cell growth on aligned TiO2 nanotubes, J. Biomed. Mater. Res. A 78A (2006) 97–103.
[107] K. Indira, U. Kamachi Mudali, N. Rajendran, Corrosion behavior of electrochemically assembled nanoporous titania for biomedical applications, Ceram. Int. 39 (2013) 959–967.
[108] S.-J. Park, S.-B. Bae, S.-K. Kim, T.-G. Eom, S.-I. Song, Effect of implant surface microtopography by hydroxyapatite grit-blasting on adhesion, proliferation, and differentiation of osteoblast-like cell line, MG-63, J. Korean Assoc. Oral Maxillofac. Surg. 37 (2011) 214–224.
[109] M.J. Jackson, W. Ahmed, Anodization: a promising nano-modification technique of titanium implants for orthopedic application, in: J.J. M, A.W (Eds.), Surface Engineered Surgical Tools and Medical Devices, 1 ed., Springer, 2007, pp. 21–47.
[110] J. He, W. Zhou, X. Zhou, X. Zhong, X. Zhang, P. Wan, B. Zhu, W. Chen, The anatase phase of nanotopography titania plays an important role on osteoblast cell morphology and proliferation, J. Mater. Sci. 19 (2008) 3465–3472.
[111] A. Dorner-Reisel, C. Schürer, C. Nischan, O. Seidel, E. Müller, Diamond-like carbon: alteration of the biological acceptance due to Ca–O incorporation, Thin Solid Films 420 (2002) 263–268.